Ali et al. *Zool. Res.* 2025, 46(3): 485−504
https://doi.org/10.24272/j.issn.2095-8137.2024.327
https://cstr.cn/32248.14.zr.2024.327

ZR | Zoological Research

Article Open Access

Phylogeography of a dominant desert lizard reveals the synergistic effects of topography and climate dynamics on diversification in arid eastern-Central Asia

Abid Ali[1,2], Da-Li Chen[3], Tatjana N. Dujsebayeva[4], Qi Song[5], Khayankhyarvaa Terbish[6], Jun Li[7], Yin Qi[1], Xian-Guang Guo[1,2,*]

[1] *Chengdu Institute of Biology*, *Chinese Academy of Sciences*, *Chengdu*, *Sichuan* 610213, *China*

[2] *University of Chinese Academy of Sciences*, *Beijing* 100049, *China*

[3] *Department of Pathogenic Biology*, *West China School of Basic Medical Sciences and Forensic Medicine*, *Sichuan University*, *Chengdu*, *Sichuan* 610041, *China*

[4] *Laboratory of Ornithology and Herpetology*, *Institute of Zoology*, *Ministry of Science and Higher Education of the Republic of Kazakhstan*, *Almaty* 050060, *Kazakhstan*

[5] *Chengdu Library and Information Center*, *Chinese Academy of Sciences*, *Chengdu*, *Sichuan* 610299, *China*

[6] *Department of Biology*, *School of Sciences and Arts*, *National University of Mongolia*, *Ulaanbaatar* 14200, *Mongolia*

[7] *College of Life Science and Technology*, *Xinjiang University*, *Urumqi*, *Xinjiang* 830046, *China*

ABSTRACT

Comprehensive phylogeographic insights require the integration of evidence across diverse taxa, ecosystems, and geographical regions. However, our understanding of the arid biota of the vast Asian drylands remains limited. Accordingly, this study combined phylogeographic analyses with ecological niche modeling to investigate patterns of diversification and demography of the Central Asian racerunner (*Eremias vermiculata*), a widespread lizard inhabiting arid eastern-Central Asia (AECA). Mitochondrial DNA (mtDNA) sequences were obtained from 876 individuals across 113 localities, while three nuclear genes—*CGNL1*, *MAP1A*, and *β-fibint7*—were sequenced from 204, 170, and 138 individuals, respectively. Analyses identified four distinct mtDNA lineages corresponding to specific geographic subregions within the AECA, reflecting the topographic and ecological heterogeneity of the region. The detection of mito-nuclear discordance indicated the presence of complex evolutionary dynamics. Divergence dating placed the initial lineage splits at approximately 1.18 million years ago, coinciding with major tectonic activity and climatic aridification that likely promoted allopatric divergence. In particular, lineage diversification within the Tarim Basin suggests that recent environmental shifts may have contributed to genetic divergence. Demographic reconstructions revealed signatures of population expansion or range shifts across all lineages during the Last Glacial Maximum, signifying the combined influence of the unique topography and climate dynamics of the AECA on diversification and demographic change. These results highlight the need for fine-scale genomic investigations to clarify the mechanisms underlying mito-nuclear discordance and local adaptation. Such efforts are essential for advancing understanding of how genetic diversity in dryland taxa responds to environmental change, providing insights into the evolutionary adaptability of species in dynamic landscapes.

Keywords: Demographic history; Ecological niche modeling; Genetic structure; Pleistocene climatic oscillations; Phylogeography

INTRODUCTION

Phylogeography represents a foundational discipline within biogeography and evolutionary genetics, providing critical insights into the spatial structuring of genetic variation among closely related species in different geoclimatic contexts (Avise, 2000). As reviewed by Avise (2009) and Hickerson et al. (2010), phylogeographic approaches are essential for

This is an open-access article distributed under the terms of the Creative Commons Attribution Non-Commercial License (http://creativecommons.org/licenses/by-nc/4.0/), which permits unrestricted non-commercial use, distribution, and reproduction in any medium, provided the original work is properly cited.

Copyright ©2025 Editorial Office of Zoological Research, Kunming Institute of Zoology, Chinese Academy of Sciences

Received: 08 January 2025; Accepted: 11 March 2025; Online: 12 March 2025

Foundation items: This work was supported by the Central Asia Drug Discovery and Development Centre of Chinese Academy of Sciences (180GJHZ2024036MI), National Natural Science Foundation of China (32070433, 32470466, 31672270, 31872959), Third Xinjiang Scientific Expedition Program (2021xjkk0600), and Special Exchange Program of the Chinese Academy of Sciences. Abid Ali was sponsored by the ANSO Scholarship for Young Talents

*Corresponding author, E-mail: guoxg@cib.ac.cn

reconstructing the evolutionary trajectories of species in relation to their geographical environments. Research has consistently demonstrated that climatic oscillations have repeatedly reorganized biota at all levels, from the genetic to the ecosystem scale (Davis & Shaw, 2001; Hewitt, 2000, 2004). The genetic, physiological, and behavioral adaptability of a species determines whether climatic change results in demographic decline or persistence and range expansion (Garcia et al., 2014). Consequently, species tend to exhibit distinct, individualistic responses to past climatic shifts (Ackerly et al., 2010; Anadón et al., 2015; Stewart et al., 2010). Furthermore, the evolutionary consequences of historical climate change have varied across different geographical locations, resulting in multifaceted, region-specific impacts (Garcia et al., 2014). This complexity presents substantial challenges for reconstructing phylogeographic history, requiring the integration of data across diverse taxa, ecosystems, geographical regions, and climatic conditions.

To date, however, most previous phylogeographic studies have focused on the temperate regions of Europe and North America, where glacial-interglacial dynamics have been extensively studied (Keppel et al., 2012). This geographic bias has left the evolutionary histories of dryland biotas comparatively underexplored, despite the crucial role of aridification—a process as pervasive and impactful as Quaternary glaciation—in shaping these regions (Byrne et al., 2008, 2018; Maestre et al., 2021). Although phylogeographic research has made substantial progress in elucidating the genetic histories of temperate species, dryland systems remain underrepresented, despite the profound evolutionary impacts of aridification, which warrant further exploration.

Drylands cover approximately 41% of the global terrestrial surface (Reynolds et al., 2007) and represent the largest terrestrial biome on Earth (Schimel, 2010). These regions provide critical ecosystem services to support growing human populations (Wang et al., 2014). Their vulnerability to degradation is exacerbated by multiple stressors, with climate change constituting a primary driver of ecological instability (Austin, 2011; Reynolds et al., 2007). Given their ecological importance and susceptibility to disturbance, drylands are central to understanding and addressing the challenges posed by ongoing global climate change. Investigating organismal responses to past climatic fluctuations offers critical insights into adaptive capacity and resilience, with implications for predicting current and future challenges (Avise et al., 2016), while also guiding the development of effective strategies to mitigate future climate impacts (Pepper & Keogh, 2021). However, such evolutionary perspectives remain limited in the dryland systems of Asia, highlighting the urgent need for expanded phylogeographic and evolutionary research in this underrepresented region.

Arid Central Asia (ACA), the largest non-zonal temperate dryland globally, spans the mid-latitudes of Eurasia and encompasses Central Asian nations, northwestern China, and Mongolia (Chen et al., 2013). This geologically and ecologically diverse region has been profoundly shaped by long-term aridification and Pleistocene glacial cycles, both of which have exerted major evolutionary pressures on regional biota (e.g., Liu et al., 2019; Melville et al., 2009; Shi et al., 2023; Wu et al., 2023). The onset of intensified aridification during the Mid-Pleistocene Climate Transition (MPT, 1.25–0.7 million years ago (Ma) was accompanied by landscape-scale ecological shifts, including the expansion of open habitats and desert-loess landscapes (Zan et al., 2024). In particular, the Taklimakan Desert, the second largest active dune field in the world, has persisted since the MPT (Fang et al., 2020; Liu et al., 2020). The desert landforms of the ACA, shaped by geological and climatic factors, have greatly influenced the distribution and evolution of its biota (Chen et al., 2013). Despite increasing interest in the genetic and evolutionary dynamics of ACA biota (e.g., Barbolini et al., 2020; Liu et al., 2019; Wang & Zhang, 2022; Wu et al., 2023; Zhang et al., 2008), the historical biogeography of many terrestrial lineages remains poorly resolved. The diverse species of the ACA offer a valuable framework for studying the effects of geographic complexity, glacial cycles, and aridification on phylogeographic structure and population dynamics, which are crucial for understanding evolutionary history and ecological adaptations in this challenging environment.

The Central Asian racerunner or variegated racerunner (*Eremias vermiculata*), a dominant desert lizard species inhabiting arid eastern-Central Asia (AECA), represents an excellent candidate for phylogeographic investigation. Characterized by restricted dispersal capacity and a broad distribution across heterogeneous arid environments, this species is well suited for exploring patterns of population divergence and historical demography (Editorial Committee of Zoology of China, Chinese Academy of Sciences, 1999; Szczerbak, 2003; Uetz et al., 2024). Adapted to desert and gravel habitats, this species is known for its “variegated” coloration and patterning—ranging from gray to yellow and black, often with contrasting spots or stripes—which provides effective camouflage in its natural habitat (Editorial Committee of Zoology of China, Chinese Academy of Sciences, 1999). Its range extends across the Zaisan Depression in Kazakhstan, Gobi Desert in southern Mongolia, and sand dunes of northwestern China (Editorial Committee of Zoology of China, Chinese Academy of Sciences, 1999; Liu et al., 2014; Szczerbak, 2003). Given its extensive range and limited mobility, this lizard provides an ideal framework for studying genetic differentiation among populations affected by dynamic landscapes. Additionally, its proximity to mountainous regions—likely serving as refugia during glacial maxima—further enhances its value as a model for examining the effects of past climatic extremes on evolutionary processes. These topographically complex systems likely enabled persistence during arid-glacial phases, promoting regional adaptation and diversification. Despite this, studies on *E. vermiculata* are scarce (Chen et al., 2019; Guo et al., 2011; Tong et al., 2016; Zhou et al., 2016), primarily due to challenges in sampling and field logistics.

To address this deficiency, extensive field sampling of *E. vermiculata* was undertaken across arid regions in China, Kazakhstan, and Mongolia to resolve patterns of genetic structure and assess the impact of geomorphological complexity and historical climatic fluctuations on lineage diversification and population dynamics. This study integrated phylogeographic analysis with ecological niche modeling to reconstruct the evolutionary history of *E. vermiculata* in the context of desert dynamics and topographic heterogeneity. Combined analysis of mitochondrial DNA (mtDNA) and nuclear DNA (nuDNA) sequences enabled detailed inference of demographic responses to paleoclimatic events, including range shifts and population expansions associated with the Last Glacial Maximum (LGM).

MATERIALS AND METHODS

Sample collection

Since 2007, extensive field surveys have been carried out to collect *E. vermiculata* samples from northwestern China and adjacent regions. A total of 878 individuals were sampled from 113 unique locations, spanning the potential geographic range of the species. Sampling encompassed 111 sites within China (designated sites 1–111), as well as one site in Kazakhstan (site 112) and one site in Mongolia (site 113). Detailed information is provided in Figure 1A and Supplementary Table S1. For each individual, the distal portion of the tail was clipped and preserved in 95% ethanol. At each site, one to three individuals were euthanized via intraperitoneal injection of sodium pentobarbital, after which voucher specimens were prepared and preserved for reference. All remaining lizards were released immediately after tail clipping at the capture site. Liver tissue samples from euthanized individuals were also preserved in 95% ethanol. All specimens and tissue samples are stored at the Chengdu Institute of Biology, Chinese Academy of Sciences, and provide a valuable resource for current and future research. Additional tissue samples were generously provided by collaborating herpetologists, with associated voucher specimens archived at Xinjiang University (China) and the University of Guelph (Canada). This collaborative, multi-institutional sampling framework provides a comprehensive resource for phylogeographic and ecological investigations of *E. vermiculata*.

DNA isolation, amplification, and sequencing

Genomic DNA was extracted from the tail and liver samples using a TIANamp Genomic DNA Kit (TIANGEN BioTech, China), following the manufacturer's recommended procedures. The extracted genomic DNA was stored at –20°C to preserve its integrity and prevent degradation. DNA quantity and quality were assessed by electrophoresis on a 1% agarose gel stained with 4S GelRed Nucleic Acid Stain (Sangon Biotech, China), and DNA concentration and purity were assessed using a NanoDrop 2000 spectrophotometer (Thermo Fisher Scientific, USA) to ensure that samples met the required standards for subsequent analyses.

Genomic DNA samples were subsequently used to amplify specific DNA fragments, including mtDNA and nuDNA loci. Two mitochondrial genes were amplified, including cytochrome oxidase 1 (*COI*, 660 bp) and cytochrome *b* (cyt *b*,

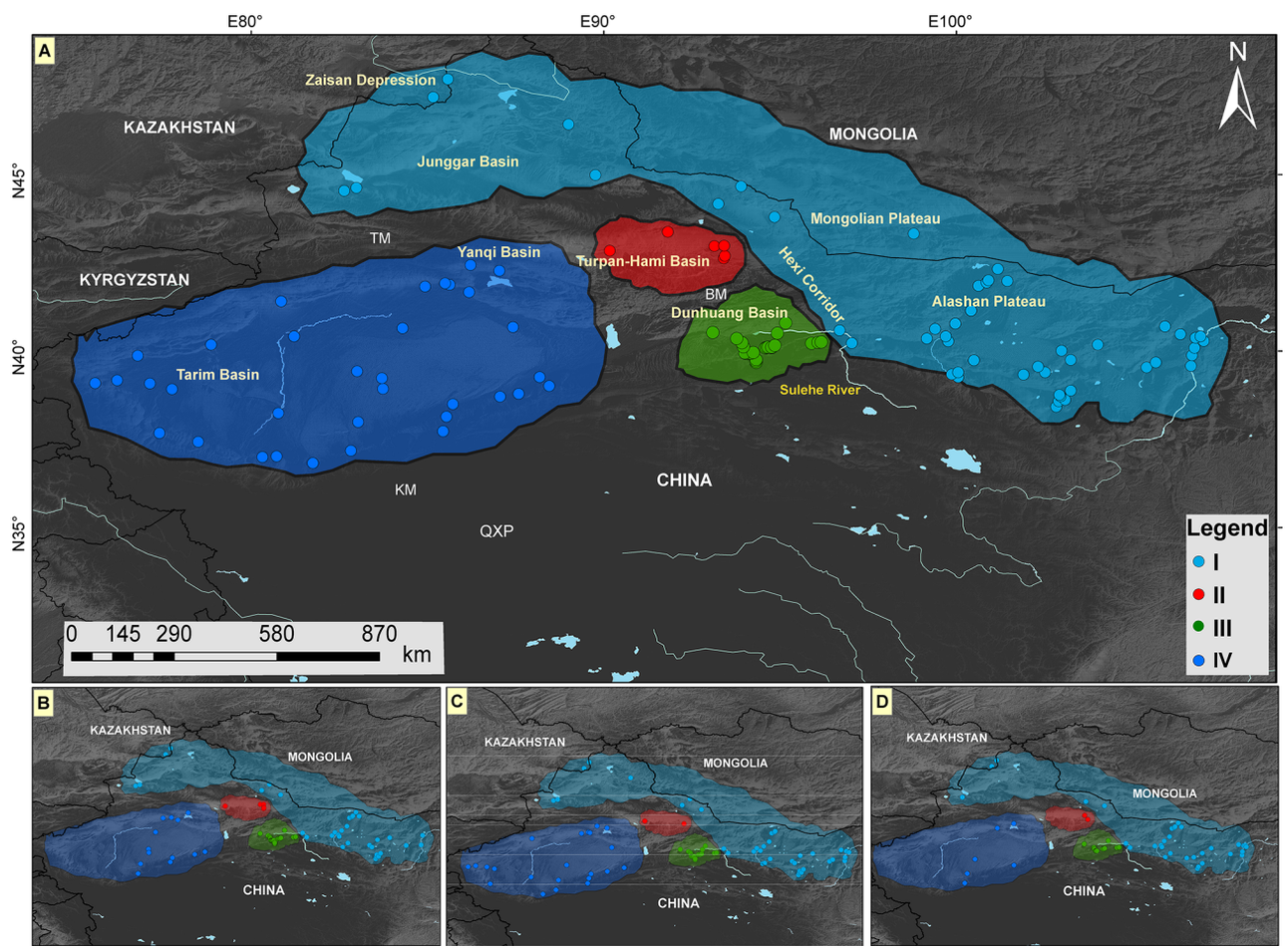


Figure 1 Distribution of *Eremias vermiculata* sampling sites in this study

A: Locations of 113 sampling sites representing 876 individuals used in the mtDNA dataset. B: Sampling sites for 204 samples of *CGNL1*. C: Sampling sites for 170 samples of *MAP1A*. D: Sampling sites for 138 samples of *β-fibint7*. Sampling sites are color-coded according to four defined geographic units. Unit I consists of the Mongolian Plateau (MP), including the Alashan Plateau, Hexi Corridor, Zaisan Depression, and Junggar Basin. Unit II covers the Turpan-Hami Basin, Unit III covers the Dunhuang Basin, and Unit IV includes the Tarim and Yanqi Basins. Major landscape features, such as the Qinghai-Xizang Plateau (QXP), Tianshan Mountains (TM), Beishan Mountains (BM), Kunlun Mountains (KM), and Sulehe River, are highlighted.

1 143 bp), from 876 individuals across all 113 sampling sites. Three nuclear DNA regions were also amplified, including cingulin-like protein 1 (*CGNL1*, 832 bp) from 204 individuals, microtubule-associated protein 1A (*MAP1A*, 1 756 bp) from 170 individuals, and β-fibrinogen intron 7 (*β-fibint7*, 659 bp) from 138 individuals, via polymerase chain reaction (PCR) (Supplementary Table S2).

To amplify both mitochondrial and nuclear genes, PCR reactions were performed in 25 μL volumes, each consisting of 12.5 μL of 2× Taq PCR Master Mix (Sangon Biotech, China), 10 μL of sterilized ultrapure water, 1 μL of each gene-specific primer, and 0.5–0.7 μL of template DNA. A comprehensive overview of the primer sets, respective base pairs, and PCR conditions for each gene is provided in Supplementary Table S2. Reactions were completed with a final extension step at 72°C for 10 min, after which the samples were cooled and stored at 4°C. PCR amplification efficacy was confirmed by electrophoresis on 1.0% agarose gels, with the PCR products subsequently sent to Sangon Biotech (China) for purification and bidirectional sequencing using an ABI 3730 automated sequencer (Applied Biosystems, USA). All sequences were deposited in GenBank under accession numbers PQ311739–PQ312606, HQ733863–HQ733868, PQ310783–PQ311658, PQ339116–PQ339319, PQ339320–PQ339489, and PQ339490–PQ339627 (Supplementary Table S1).

Sequence alignment and phylogenetic analyses

Sequence alignment was performed in MEGA v.11.0 (Tamura et al., 2021) using the MUSCLE algorithm with default settings. Concatenation of the *COI* and cyt *b* gene segments was conducted using SeaView v.5.0.5 (Gouy et al., 2010). Sequences were carefully checked, especially at polymorphic sites, and translated into amino acids to ensure sequencing accuracy. Unique haplotypes in the aligned matrix were identified using DnaSP v.6.12.03 (Rozas et al., 2017). The phasing approach (Stephens et al., 2001; Stephens & Donnelly, 2003) was applied using the DnaSP package to resolve any ambiguities in base pairs in the nuclear gene data. Phase reconstruction was unambiguous, with phase probabilities of at least 0.95 at all heterozygous sites.

Phylogenetic relationships among mitochondrial haplotypes were reconstructed using a concatenated dataset of *COI* (660 bp) and cyt *b* (1 143 bp) sequences. Two robust methods were employed to infer phylogeny and assess node support, including Bayesian inference (BI) with MrBayes v.3.2.2 (Ronquist et al., 2012) and maximum-likelihood (ML) with IQ-TREE v.1.6.7 (Nguyen et al., 2015). To improve the accuracy of phylogenetic inference, the concatenated dataset was partitioned by codon position (1st, 2nd, and 3rd) for each gene to accommodate variation in substitution rates across sites. PartitionFinder v.2.1.1 (Lanfear et al., 2017) was used to identify the optimal partitioning scheme and best-fitting nucleotide substitution models under corrected Akaike information criterion (AICc) (Supplementary Table S3). In the absence of a clearly defined sister taxon for *E. vermiculata*, two closely related species, *E. velox* and *E. przewalskii*, were selected as outgroups based on Chen et al. (2019), with their mtDNA datasets retrieved from GenBank (Supplementary Table S1). BI analysis was conducted using two independent runs, each consisting of four Monte Carlo Markov chains (MCMCs) executed for 20 000 000 generations, with parameters and topologies sampled every 1 000 generations. Convergence between runs was assessed based on the standard deviation of split frequencies (<0.01) and an effective sample size (ESS) exceeding 200, calculated using Tracer v.1.7.1 (Rambaut et al., 2018). After discarding the first 25% of sampled trees as burn-in, a 50% majority-rule consensus tree was generated with posterior probabilities (PP) assigned to each node. ML analysis was performed under the same partition-specific models, with branch support assessed using ultrafast bootstrap approximation (UFBoot) with 5 000 replicates. Nodes with UFBoot values above 95% were considered well-supported (Minh et al., 2013). Phylogenetic trees were visualized and refined using FigTree v.1.4.4 (Rambaut, 2016). MEGA was used to calculate the mean genetic distance between lineages using uncorrected *p*-distances.

Haplotype networks were constructed using both mitochondrial and nuclear datasets through median-joining network (MJN) analysis in NETWORK v.4.6.1.3 (Bandelt et al., 1999; http://www.fluxus-engineering.com/). This approach enabled the inference of genealogical relationships among haplotypes and their spatial distribution patterns, offering a detailed framework for assessing lineage connectivity and geographic structuring in *E. vermiculata*.

Divergence time estimation

BI was used to estimate divergence times of major lineages using BEAST v.1.8.4 (Drummond et al., 2012) to reconstruct the temporal framework of lineage diversification in *E. vermiculata* based on mtDNA. In the absence of a definitive fossil record for direct calibration, a two-step secondary calibration strategy was adopted, similar to the strategy used by Brandley et al. (2010), to ensure robust temporal estimates. The first step involved assembling a dataset of 135 sequences from NCBI (https://www.ncbi.nlm.nih.gov/), covering a range of species within the family Lacertidae (Supplementary Table S4). This dataset included one representative sequence from each lineage of *E. vermiculata* identified by ML and BI analyses. This integrated dataset was then used to estimate the age of the most recent common ancestor (MRCA) of *E. vermiculata.* Prior to conducting dating analysis, PartitionFinder v.2.1.1 (Lanfear et al., 2017) was used to identify the optimal partitioning scheme and substitution models under AICc. Divergence dating was then conducted under a relaxed lognormal molecular clock model in BEAST (Supplementary Table S3). Eight calibration points were applied, each defined by a normal distribution probability density. The first calibration point (C1) was the MRCA of the subfamily Lacertinae, calibrated to13.75±0.01 Ma, based on Pavlicev & Mayer (2009). The second calibration point (C2), representing divergence within *Takydromus*, was set at 5.2±0.9 Ma (Tseng et al., 2014). Additional calibrations (C3 to C8) were incorporated based on Tamar et al. (2016), relevant to other lacertid genera, as well as *Gallotia* and *Podarcis.*

In the second step, divergence times among intraspecific lineages of *E. vermiculata* were estimated using all available mtDNA sequences. This analysis was anchored to the previously established age estimate for the MRCA of *E. vermiculata* (1.19±0.3 Ma), derived from our initial assessment (Supplementary Figure S1). PartitionFinder was again used to define the most appropriate partitioning schemes and corresponding evolutionary models under AICc (Lanfear et al., 2017). Analyses were performed using a relaxed lognormal clock in BEAST and two alternative tree priors: a birth-death

process and a constant-size coalescent model. This approach ensured that the choice of tree prior did not bias the molecular dating results, as recommended by Ritchie et al. (2017). Tracer v.1.7.1 was employed to check that all parameters reached an ESS greater than 200, indicating sufficient convergence (Rambaut et al., 2018). Model parameter convergence was rigorously assessed using both Tracer and TreeAnnotator, essential tools in BEAST, which generated maximum credibility trees with mean divergence times and 95% highest posterior density (HPD) intervals. The first 25% of trees were discarded as burn-in to ensure that only the stationarity phase of the MCMC was retained. To evaluate the fit of different partitioning strategies, Bayes factors (BF) were calculated using the 2lnB10 equation (Newton & Raftery, 1994) in Tracer v.1.4 (Rambaut & Drummond, 2007). A BF greater than 10 was interpreted as strong support for the more partitioned model, following the criteria of Kass & Raftery (1995). Detailed information on models, priors, and parameters is provided in Supplementary Table S3.

Population genetic analyses

To determine the impact of haplotype differences on population differentiation in *E. vermiculata*, comprehensive genetic diversity analysis was performed using DnaSP v.6.12.03 (Rozas et al., 2017). Key summary statistics were computed for each lineage, including the number of haplotypes (n_h), haplotype diversity (H_d), nucleotide diversity (π), and average number of nucleotide differences (k). The spatial distribution of genetic diversity across four primary lineages (I, II, III, and IV) of *E. vermiculata* was also determined. This categorization was based on the phylogeographic delineations derived from both BI and ML analyses. To quantify genetic structure among these lineages, analysis of molecular variance (AMOVA) was performed using Arlequin v.3.5 (Excoffier & Lischer, 2010). This hierarchical approach allowed partitioning of genetic variation within and among groups, thereby revealing patterns of lineage-level differentiation. To further explore the genetic substructure within Lineage IV, samples were subdivided into western and eastern groups, corresponding to distinct clusters identified in the MJN (Supplementary Figure S2). Statistical significance of variance components was tested using 1 000 permutations, providing a rigorous assessment of population-level genetic structure.

Isolation by resistance, distance, and environment

To assess the relative contributions of landscape resistance, geographic distance, and environmental factors to genetic differentiation in *E. vermiculata*, complementary frameworks of isolation by resistance (IBR; McRae, 2006), distance (IBD; Wright, 1943), and environment (IBE; Wang & Bradburd, 2014) were applied using different approaches. Sampling localities (n=113) were consolidated into 100 spatially grouped sites to capture regional patterns and minimize redundancy. Pairwise genetic distances (p-distances) were computed using MEGA and served as the response matrix in subsequent analyses.

To evaluate the role of mountainous terrain in restricting gene flow through IBR, elevation was selected as the primary predictor of landscape resistance, informed by field observations indicating that *E. vermiculata* predominantly occupies habitats below 2 100 m a.s.l. Elevation data were downloaded from the WorldClim website (worldclim.org/data/worldclim21.html) and cropped to the spatial extent defined by the ecological niche model (ENM). Given that high-altitude regions are expected to act as dispersal barriers for lowland-adapted taxa, elevation was transformed into continuous resistance surfaces. Landscape resistance was modeled using the ResistanceGA package (Peterman, 2018), which employs a genetic algorithm to optimize resistance values based on genetic diversity measurements. The inverse Ricker transformation was applied to the elevation data to generate resistance surfaces, following the method applied by Chang et al. (2022). Surface optimization was performed twice using the GA.prep and SS_optim functions (Peterman, 2018). Final pairwise resistance distances, expressed as random-walk commute times and equivalent to CIRCUITSCAPE "resistance distance" (McRae et al., 2008), were calculated using the CommuteDistance function in the gdistance R package (van Etten & Hijmans, 2010).

Euclidean geographic distances for the IBD model were computed using GeographicDistanceMatrixGenerator v.1.2.3 (Ersts, 2024). To assess IBE, 19 contemporary bioclimatic variables were extracted from WorldClim v.1.4 (http://www.worldclim.org, accessed on 22 November 2023) at each sampling coordinate using ArcGIS v.10.8. To reduce redundancy and control for multicollinearity, variance inflation factor (VIF) analysis was performed using the usdm package in R (Naimi et al., 2014), excluding variables with correlations above a threshold of 10. The selected variables are listed in Supplementary Table S5. Environmental Euclidean distances between sample points were determined using the vegan package in R (Dixon, 2003).

Model selection and hypothesis testing were performed using the Maximum Likelihood Population-Effects model (MLPE; Clarke et al., 2002) and Multiple Regression on Distance Matrices (MRDM; Goslee & Urban, 2007). MLPE modeling was implemented via the MLPE.lmm function in the ResistanceGA package (Peterman, 2018), with model performance evaluated using AIC and Bayesian Information Criterion (BIC). To evaluate the relative influence of resistance, geographic, and environmental distances on genetic differentiation, MRDM analysis was conducted using the MRM function in the ecodist package, following the methodology of Jiao et al. (2024). Pairwise genetic distance served as the response variable, and the predictor variables included all three distance types. Four MRM models were tested, including a full model incorporating all three distances and separate models testing each predictor individually. For each model, 10 000 permutations were used to assess statistical significance.

Inference of demographic histories

Historical population dynamics of *E. vermiculata* were reconstructed using a trio of mtDNA-based analytical approaches to investigate fluctuations within the I, II, III, and IV lineages delineated in the phylogenetic analyses. Prior to demographic inference, the most appropriate evolutionary model for each lineage-specific dataset was determined using PartitionFinder v.2.1.1 (Lanfear et al., 2017) under the AICc (Supplementary Table S3). Temporal patterns of population size change were inferred using Bayesian skyline plots in BEAST v.1.10.4 (Suchard et al., 2018). Each lineage was analyzed under a strict molecular clock, calibrated with a mean substitution rate of 0.046 substitutions per site per million years, as estimated from divergence dating. Model configurations, priors, and parameters are outlined in

Supplementary Table S3. The resulting plots were visualized and assessed using Tracer v.1.7 (Rambaut et al., 2018). Bayesian skyline estimates were complemented by Tajima's *D* (Tajima, 1989) and Fu's *Fs* (Fu, 1997) using Arlequin v.3.5 (Excoffier & Lischer, 2010), along with their respective *P*-values based on 10 000 simulated samples. These statistics can detect population expansion signals in mtDNA datasets, offering robust power across various scenarios, including larger (Fu's *Fs*) and smaller sample sizes (Tajima's *D*). Mismatch distribution (MD) analyses were also conducted to examine the distribution of pairwise nucleotide differences for each lineage using Arlequin v.3.5 (Excoffier & Lischer, 2010), providing insight into the historical demographic processes, particularly sudden changes in population size. Bar plots were generated using the R package to compare the expected and observed values of MD. Goodness-of-fit between these observed and expected distributions was rigorously tested using Harpending's Raggedness Index (Harpending, 1994) and the Sum of Squared Deviation (*SSD*). The fit of the observed data was tested against a null distribution of constant population size using the R_2 statistic of Ramos-Onsins & Rozas (2002) and 10 000 coalescent simulations in DnaSP. A significantly positive R_2 value was interpreted as evidence of population expansion.

Ecological niche modeling

To assess habitat suitability across past, present, and projected future climates, bioclimatic variables were obtained from WorldClim v.1.4 (Hijmans et al., 2005), a comprehensive global climate database. Our analysis spanned five major climatic intervals, including the Last Interglacial (LIG; ~0.14–0.12 Ma), Last Glacial Maximum (LGM; ~0.02 Ma), mid-Holocene (MH; ~6 000 years ago), present-day (1960–1990), and a future scenario representing the 2070s (2061–2080). Each dataset was harmonized to a uniform spatial resolution of 2.5 arcmin for consistent comparison. Paleoclimatic reconstructions for the LGM and MH were derived from climate simulations from the Model for Interdisciplinary Research on Climate (MIROC-ESM) (Watanabe et al., 2011), selected for its performance in simulating past climate dynamics. Future climate projections were based on the MIROC6 model under the Shared Socio-economic Pathways (SSP 245/585) scenario, providing a nuanced perspective on potential climate conditions influenced by different socio-economic factors.

ENMs for *E. vermiculata* were developed using MAXENT v.3.4.1 (Phillips et al., 2006), accessed via the 'SDM' package in R (Naimi & Araújo, 2016). A total of 171 occurrence records for *E. vermiculata* were compiled, including 113 unique observations from our field surveys, 21 records from the Global Biodiversity Information Facility (GBIF), and 37 observations extracted from published literature. All GPS occurrence points were manually verified to eliminate duplicate or erroneous records. To improve model accuracy, occurrences from the Mongolian plateau, including those from the Gobi Desert, were specifically assigned to Lineage I. To reduce spatial sampling bias, SDMtoolbox v.2.0 (Brown et al., 2017) in ArcGIS was used to ensure that no two locations were within 10 km of each other. This process resulted in a refined dataset of 136 records spanning the entire study area, which was used for final ENM analysis (Supplementary Table S6).

To minimize the confounding effects of multicollinearity on ENM predictive accuracy, pairwise Pearson correlation coefficients were calculated for all 19 bioclimatic variables using the "psych" package in R (Revelle, 2017) (see Supplementary Figure S3 for the correlation matrix). Variables with a correlation coefficient (r) greater than 0.6 were excluded from analysis to ensure independence among predictors. This rigorous selection process resulted in the inclusion of five key variables for ENM, including bio2 (Mean Diurnal Range), bio4 (Temperature Seasonality), bio13 (Precipitation of Wettest Month), bio14 (Precipitation of Driest Month), and bio19 (Precipitation of Coldest Quarter).

Species-level ENM is a widely recognized approach (Qiao et al., 2017; Smith et al., 2019), based on the principle of "niche conservatism" (Peterson et al., 1999), which suggests that species respond consistently to climatic drivers and maintain similar ecological niches across different spatial and temporal scales. However, recent research has highlighted the importance of finer-scale taxonomic resolution in capturing specific ecological contexts (Pearman et al., 2010; Serra-Varela et al., 2015; Smith et al., 2019).

To account for both broad-scale and lineage-specific ecological differentiation in *E. vermiculata*, a multi-scale modeling framework was adopted. Niche models were constructed at two taxonomic levels: (1) species level, treating all occurrences as a single entity, and (2) lineage level, focusing on lineages I and IV, which were represented by 79 and 37 localities, respectively. This dual-scale approach enabled detection of subtle differences in habitat suitability and facilitated a deeper understanding of the ecological dynamics within and between these lineages. Maxent modeling was conducted using 70% of the occurrence data for training and 30% for validation, with 100 replicates generated via subsampling and a maximum of 5 000 iterations per run. Model performance was assessed using the area under the receiver operating curve (AUC-ROC) and the true skill statistic (TSS). The significance of each variable was also evaluated, providing insights into the key drivers of habitat suitability for *E. vermiculata* and its distinct lineages. This comprehensive approach ensured a nuanced understanding of the ecological requirements of the species and its response to environmental changes.

Niche overlap between lineages

To assess the degree of climatic niche overlap among *E. vermiculata* Lineages I, III, and IV (with adequate sampling sites), niche similarity analyses were conducted using the framework developed by Broennimann et al. (2012). Climatic niche differentiation was further explored using the PCA-env approach (Broennimann et al., 2012) implemented in the "ecospat" package in R (Di Cola et al., 2017). Our analysis utilized the same number of occurrence points as used in the ENMs for Lineages I and IV, and included an additional 13 occurrence points from the Dunhuang Basin for Lineage III to improve assessment. All analyses were conducted with the same environmental variables and spatial extent (Zone M) as used in the ENM.

Environmental variables associated with each occurrence point were extracted, and principal component analysis (PCA) was conducted. The first two principal components were transformed into densities by applying kernel smoothers (Di Cola et al., 2017), enabling quantification of niche overlap along PCA gradients and identification of ecological distinctiveness between the lineages. Niche overlap between

lineage pairs was measured using Schoener's *D* (*D*) and Hellinger's *I* (*I*) indices, both scaled from 0 to 1. These indices indicate the degree of divergence or convergence in climatic niches between species or lineages, with 0 indicating no overlap (completely dissimilar niches) and 1 indicating complete overlap (identical niches) (Warren et al., 2008). This analysis determined the degree of niche similarity between the compared lineages, relative to what would be expected by chance, using null models.

A deviation from the niche equivalency hypothesis—implying that lineage niches are ecologically distinct—is indicated when the observed niche overlap lies outside the 95% confidence interval of the null distribution (Fick & Hijmans, 2017). A niche similarity test was conducted to determine whether the lineage niches were more similar than expected based on the principles of conservationism or plasticity. If the observed *D* value exceeded the 95% threshold of the simulated values, this indicated niche similarity (conservation) and the null hypothesis was rejected. Statistical significance was determined based on 100 randomizations, with 1 000 permutations performed for each analysis. The test was performed on the *D*-value at an alpha level of 0.05. All pairwise comparisons were performed using a shared background extent encompassing the full study area, ensuring a robust and comprehensive comparison of ecological niches.

RESULTS

Phylogenetic analyses

A total of 362 unique haplotypes were identified across the dataset, including those corresponding to the two outgroups. Phylogenetic reconstruction of *E. vermiculata*, derived from both BI and ML analyses, was consistent and yielded four geographically distinct lineages: I, II, III, and IV. Each lineage was associated with a specific biogeographic region (Figure 1). Lineage I encompassed populations from the Alashan region, Hexi Corridor, Gobi Desert, Junggar Basin, and Zaisan Depression. Lineage II consisted of many haplotypes from the Turpan-Hami Basin, while Lineage III represented a unique genetic cluster from the Dunhuang Basin. Lineage IV was mainly characterized by haplotypes from the Tarim Basin, with additional representation from the adjacent Yanqi Basin. Notably, no haplotypes were shared across these geographic areas, indicating pronounced phylogeographic discontinuities.

Mitochondrial phylogenetic trees of *E. vermiculata* are shown in Figure 2A. Lineage-level monophyly received strong statistical support under both BI (posterior probability=1.00) and ML (bootstrap values ranging from 89% to 100%). Specifically, support values for Lineages I–IV were 1.00/100%, 1.00/92%, 1.00/89%, and 1.00/91%, respectively. Pairwise uncorrected *p*-distances between lineages ranged from 0.014 to 0.048, with a mean of 0.036 (Supplementary Table S7), further corroborating their genetic distinctiveness.

Median-joining haplotype networks based on mtDNA revealed four distinct clusters (Figure 2B), corresponding to the major lineages and their respective geographic units (Figure 1). Two substructures were identified within the Tarim Basin: western and eastern substructures (Supplementary Figure S2). Samples from the western Tarim Basin clustered into the western substructure, while those from the eastern Tarim Basin and Yanqi Basin formed the eastern substructure. In contrast, the nuDNA network exhibited a complex pattern of overlapping genetic structures between different geographic regions. Analysis of the *CGNL1* gene showed haplotype overlap between the Dunhuang and Turpan-Hami Basins, suggesting either historical gene flow and/or retention of ancestral polymorphisms between these regions and within the Mongolian Plateau and Junggar Basin. Furthermore, haplotypes from the Dunhuang Basin showed genetic similarities to those from the Tarim and Yanqi Basins. Similarly, the *MAP1A* and *β-fibint7* datasets showed haplotype sharing across all four major regions, indicating potential mito-nuclear discordance (Figure 3).

Molecular dating

Divergence time estimates derived from the secondary calibration datasets are presented in Supplementary Figure S1. The split between the MRCA of *E. vermiculata* and its closest related outgroup species occurred approximately 14.27 Ma, with a 95% HPD interval spanning 11.85–16.97 Ma. The MRCA of *E. vermiculata* was inferred to have emerged during the Middle Pleistocene, around 1.18 Ma (95% HPD: 0.46–1.68 Ma) (Figure 4). This node was subsequently used to calibrate intraspecific divergence analyses across mtDNA lineages. Comparative analyses under two distinct tree priors—birth-death and constant-size coalescent—yielded congruent results. However, BF analysis (Kass & Raftery, 1995) strongly favored the constant-size coalescent model over the birth-death model (2lnBF>−28.846), which was therefore retained as the preferred model for downstream interpretation.

Further divergences within *E. vermiculata* occurred during the late Pleistocene. Divergence between Lineages I and II was estimated at approximately 0.47 Ma (95% HPD: 0.07–0.72 Ma), while Lineages III and IV separated at approximately 0.45 Ma (95% HPD: 0.05–0.75 Ma) (Figure 4). These temporal estimates provide a robust evolutionary framework for understanding lineage diversification and highlight the historical processes that have shaped the genetic diversity and geographic distribution of *E. vermiculata*.

Molecular diversity and population genetic structure

Genetic diversity metrics for *E. vermiculata*, including number of haplotypes (*nh*), haplotype diversity (*Hd*), mean nucleotide diversity (π), and mean number of nucleotide differences (*k*) for each lineage, are summarized in Supplementary Table S8. Across the full mitochondrial dataset, nucleotide and haplotype diversities were 0.026 and 0.971, respectively. However, substantial variation was observed among lineages. Lineage I exhibited the lowest nucleotide diversity (π=0.00133), while Lineage II recorded the highest value (π=0.006), indicating notable heterogeneity in regional genetic variation. AMOVA conducted using the BI and ML phylogenetic trees revealed that 84.65% of the total genetic variation was attributed to differences among the four main groups. Variation among populations within lineages accounted for 8.3%, while within-population variation accounted for 6.97% (Supplementary Table S9). This pronounced among-group differentiation reflects strong population structure and limited gene flow across major geographic regions. Additional AMOVA focusing on the western and eastern substructures within the Tarim and Yanqi Basins, indicated that 50.8% of the genetic variation was due to differences between these groups. Genetic diversity among populations within these subgroups and the populations themselves was 18.5% and 30.5%, respectively. These results

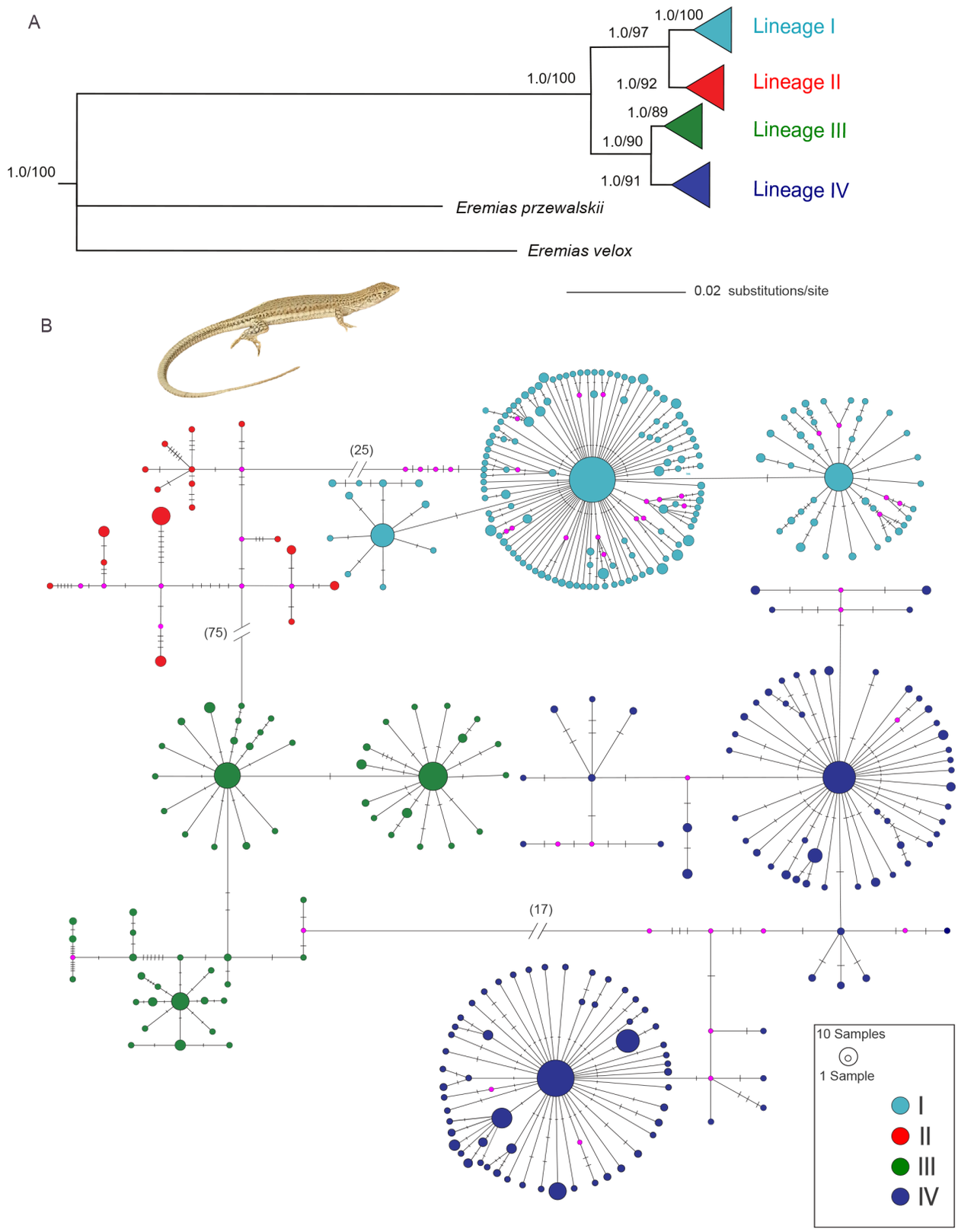


Figure 2 Phylogenetic tree and haplotype networks inferred from mtDNA dataset

A: Phylogenetic tree constructed from concatenated mtDNA sequences, with nodes indicating Bayesian posterior probability (PP)/maximum-likelihood ultrafast bootstrap (UFBoot) values. Four major lineages (I, II, III, and IV) were identified, with branch colors and shapes corresponding to geographic units in Figure 1. B: Median-Joining Network (MJN) haplotype network for concatenated mtDNA sequences. Each pie chart represents a unique haplotype, with segment colors corresponding to geographic units in Figure 1 (I: Mongolian Plateau; II: Turpan-Hami Basin; III: Dunhuang Basin; IV: Tarim and Yanqi Basins). Pie chart sizes are proportional to haplotype frequencies. Each bar crossing a network branch indicates a single substitution, with numbers indicating substitutions greater than 15. Small pink solid circles represent intermediate or unsampled haplotypes. Lizard photo by Xian-Guang Guo.

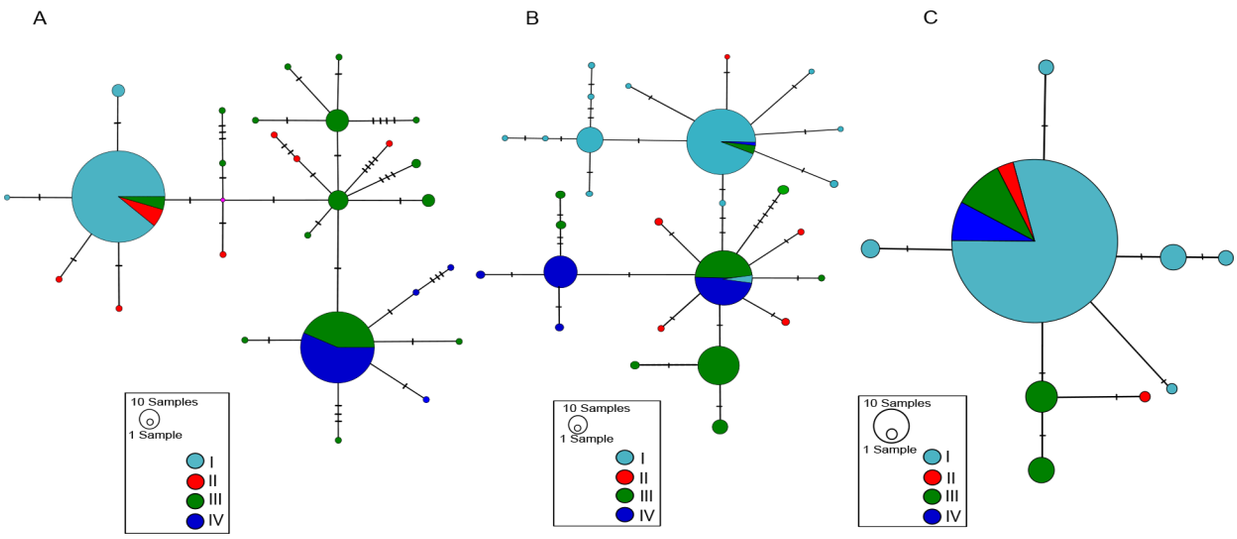


Figure 3 Median-joining networks based on three nuclear genes

A: Sequence data for all individuals from *CGNL1*. B: Sequence data for all individuals from *MAP1A*. C: Sequence data for all individuals from *β-fibint7*. Each pie chart represents one haplotype, and circle sizes represent the approximate number of individuals. Each bar crossing a network branch indicates inferred nucleotide substitutions between haplotypes. Geographical origin of haplotypes is indicated by locality colors used in Figure 1.

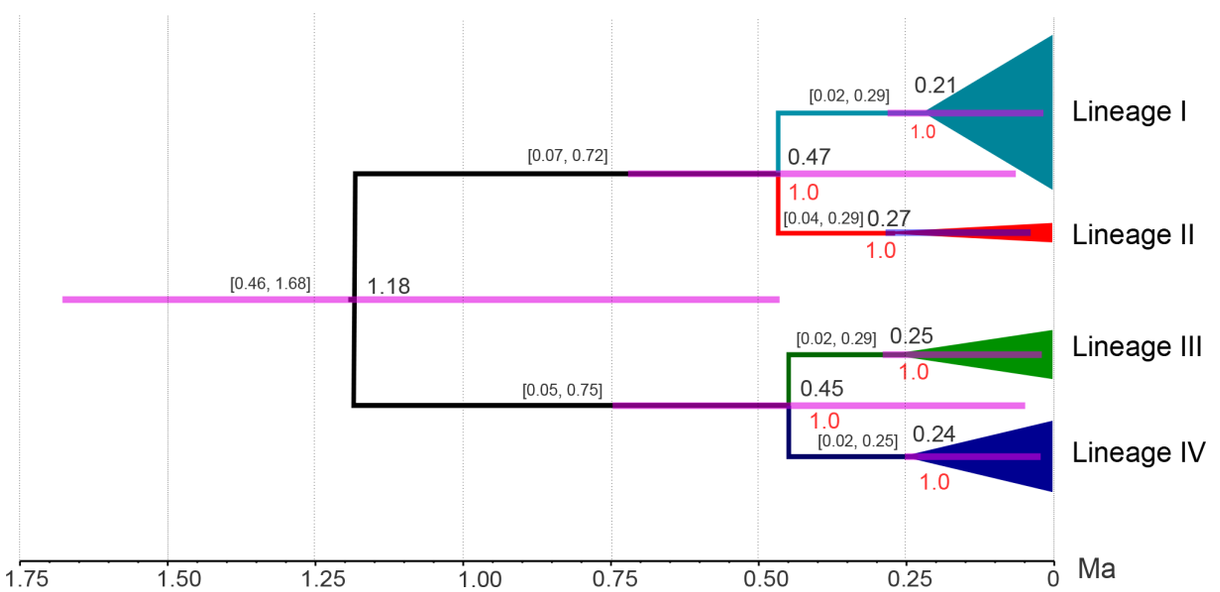


Figure 4 Chronogram of *Eremias vermiculata* based on the mtDNA dataset with a constant-size coalescent tree prior

Black numbers above nodes represent estimated mean divergence time, red numbers below nodes represent posterior probability, and pink bar represents 95% HPD for divergence time.

emphasize the importance of incorporating both broad-scale phylogeographic patterns and finer-scale population-level structure in assessments of genetic diversity and connectivity in *E. vermiculata*.

Impact of resistance, geographical, and environmental distances on genetic differentiation

MLPE and MRDM analyses were used to assess the influence of resistance, geographical, and environmental distances on genetic variance. The MLPE model comparisons revealed that IBR, IBD, and IBE models yielded similar AIC and BIC values. The IBR model had slightly lower AIC (−23 014.89) and BIC (−22 988.94) values, indicating a slightly better model fit. However, the small magnitude of these differences (Supplementary Table S10) suggests that all three models are comparably plausible within the MLPE framework. In contrast, MRDM analysis produced more differentiated results. The combined model (IBR, IBD, and IBE) jointly accounted for a modest proportion of the variation in genetic differentiation (R^2=0.194, P=0.0001), indicating that the combined effects of resistance, distance, and environment contribute to population genetic differentiation. When tested individually, IBR had a minimal effect (R^2=0.0038, P=0.003), while IBD emerged as the strongest predictor (R^2=0.1936, P=0.0001), with a similar R^2 to the combined model. These results suggest that while landscape resistance plays a role in genetic differentiation, its contribution is relatively minor compared to that of IBD. Finally, IBE exhibited no significant effect on genetic differentiation, suggesting that environmental factors do not substantially influence population differentiation in *E. vermiculata* (Supplementary Table S10).

Historical demography

Demographic reconstructions of *E. vermiculata* revealed a consistent effective population size across all lineages throughout the LGM. Based on BSP analysis, Lineage I exhibited a population expansion around 20 000 years ago, indicating sustained growth from the LGM to present day. Notable demographic shifts were also observed within Lineages III and IV, which showed substantial expansions commencing approximately 15 000 years ago, with both maintaining elevated effective population sizes into the Holocene. Notably, Lineage IV underwent a sharp population decline from 15 000 years onwards. In contrast, Lineage II exhibited more dynamic temporal variation, with a modest expansion around 50 000 years ago, followed by sustained growth during the LGM and a subsequent contraction beginning around 10 000 years ago (Figure 5A).

Neutrality test statistics further supported these demographic trends. Notably, strong negative values for both Tajima's *D* (−2.68349, *P*<0.001) and Fu's *Fs* (−26.39546, *P*<0.001) were observed in Lineage I, indicating possible demographic expansion. These results were corroborated by a low R_2 value of 0.007, pointing to genetic variation within this lineage. Similarly, Lineage IV had significantly negative values for Tajima's *D* (−2.51139, *P*<0.001) and Fu's *Fs* (−24.72596, *P*<0.001), with a positive R_2 value of 0.0175, suggesting demographic expansion. For Lineages II and III, although Tajima's *D* and Fu's *Fs* values were negative and statistically significant (II: −0.26093, −24.5325, *P*<0.001; III: −1.92496, −25.44285, *P*<0.001), indicating demographic expansion, Lineage II had a higher R_2 value (0.1018) compared to Lineage III (Supplementary Table S8). These findings suggest a scenario of demographic expansion across all lineages, with Lineage II potentially exhibiting slightly higher genetic variation.

MD analyses provided additional support for recent expansion in Lineage I, as indicated by the typical smooth unimodal distribution (Figure 5B), characterized by low and significant SSDs but non-significant *Rg* values (Supplementary Table S8). In contrast, Lineages II, III, and IV were characterized by multimodal, erratic MDs with non-significant *Rg* values, further suggesting a scenario of demographic expansion. These results provide valuable insights into the demographic history and genetic variation of *E. vermiculata* and its different lineages.

Temporal changes in suitable distributional areas

Predicted changes in the potentially suitable distribution (PSD) areas of *E. vermiculata* across historical, current, and future climatic scenarios are illustrated in Figure 6A. ENMs developed for the LIG, LGM, MH, present day, and future projections under SSP 245/585 demonstrated robust predictive performance, with mean AUC and TSS values of 0.91 and 0.74, respectively. Current suitability projections largely coincide with empirical occurrence records, confirming the distribution ranges observed during field surveys and reported in other sources.

Among the 19 bioclimatic variables evaluated, bio13 (38.7%), bio4 (18.1%), and bio19 (11.4%) contributed most significantly to the model, collectively explaining 67.5% of the variation (Supplementary Table S11). Temporal reconstructions revealed notable shifts in suitable habitat. During the LIG, potentially suitable habitats were severely restricted, with only fragmented refugia persisting. Conversely, the LGM was characterized by notable range expansion, particularly into the northern and southeastern parts of the Gobi Desert, with a pronounced southeastward shift towards the Mongolian Plateau and Turpan Depression. By the mid-Holocene, the suitable range extended westward from the northern and southeastern Gobi Desert into the Tarim Basin, traversing the Dunhuang and Turpan-Hami Basins. Currently, the suitable range for *E. vermiculata* extends across the Gobi Desert along the China-Mongolia border, including the Badain Jaran Desert, and into the Hexi Corridor, Turpan-Hami Basin, Dunhuang Basin, and entire Tarim Basin. Future projections under the SSP 245 and SSP 585 scenarios suggest a slight southwestward expansion in the Tarim Basin, although the broader spatial trends remain uncertain. Overall, the PSD areas of *E. vermiculata* show a general expansion from the northeastern Gobi Desert towards the Tarim Basin across all time periods studied, reflecting dynamic shifts in habitat suitability over time.

The PSD areas for Lineages I and IV across all time periods are depicted in Figure 6B, C, respectively. These ecological niche models showed high accuracy, with AUC values of 0.91 and 0.95 and TSS values of 0.74 and 0.86 for Lineages I and IV, respectively. Current predicted ranges closely matched known occurrences, supporting the reliability of lineage-level models. In Lineage I, bio13 (Precipitation of Wettest Month, 41%), bio4 (Temperature Seasonality, 18%), and bio2 (Mean Diurnal Range, 11%) were the principal contributors, accounting for 70% of the explanatory power of the model. For Lineage IV, the most influential variables were bio13 (68.5%), bio19 (Precipitation of Coldest Quarter, 7.6%), and bio4 (5.7%), with a cumulative contribution of 81.8% (Supplementary Table S11).

Temporal projections showed that Lineage I occupied limited suitable habitat from the LIG to the MH, with partial suitability in the Zaisan Depression, western Tarim Basin, and Gobi Desert during the LIG. Since then, its range expanded across the southeastern Gobi and into the southern Junggar Basin. Future projections indicate continued stability in this distribution. Lineage IV exhibited a different historical trajectory. No suitable habitat was identified during the LIG, but a substantial range emerged during the LGM, spanning the Mongolian Plateau, Junggar Basin, and northern Tarim Basin. The MH brought regional contraction in the north but expansion in the southeastern Gobi Desert. A subsequent shift was observed along the western margin of the Tarim Basin. Present and future projections show a stable distribution encompassing the full Tarim Basin, the Turpan Depression, and parts of the Dunhuang Basin. Together, these findings highlight the historical and projected distribution patterns of Lineages I and IV and provide a valuable framework for understanding the ecological resilience and potential responses of the species under future environmental change.

Niche overlap

Climatic niche analyses revealed distinct environmental associations among the major lineages of *E. vermiculata* (Figure 7A), with PCA indicating that PC1 (47.39%) and PC2 (21.09%) together accounted for 68.48% of the variance in environmental parameters across lineage pairs I vs. III, I vs. IV, and III vs. IV (Figure 7B).

Quantitative assessments indicated low niche overlap between Lineage I and Lineages III and IV (Table 1), with

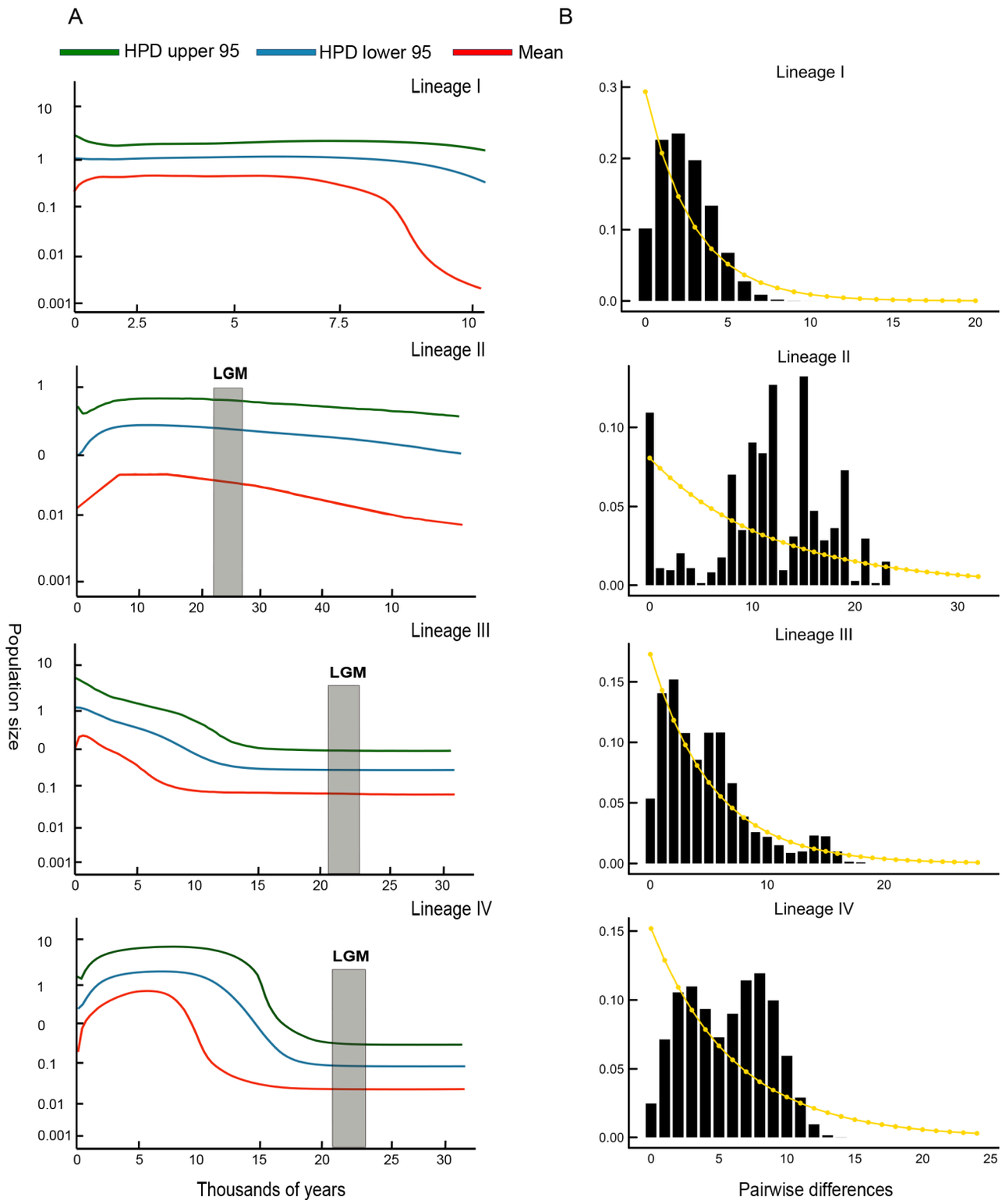


Figure 5 Demographic analyses of each *Eremias vermiculata* lineage based on mtDNA dataset

A: Bayesian Skyline Plots for each lineage. Y-axes represent estimated effective population size on a logarithmic scale ($Ne \times \tau/10^6$, product of the female effective population size and generation length in years); x-axes represent thousands of years ago. Vertical dark-gray bars represent duration of the LGM. B: Mismatch distribution analyses for each lineage. Black bars represent observed pairwise differences in distribution, and yellow lines represent theoretically expected distribution under a population expansion model.

Schoener's *D* values of 0.118 and 0.353 and Warren's *I* values of 0.253 and 0.506, respectively (Table 1). These results imply that Lineage I occupies more ecologically distinct niches compared to Lineages III and IV. However, niche equivalency tests failed to detect significant differences in niche identity among lineage pairs, with *P* values exceeding α=0.05 for all pairs (Lineage I vs. III: *P*=1; I vs. IV: *P*=0.828; III vs. IV: *P*=0.955) (Figure 8A). Thus, the null hypothesis of niche equivalency could not be rejected, indicating that any observed differences in niche occupation were statistically

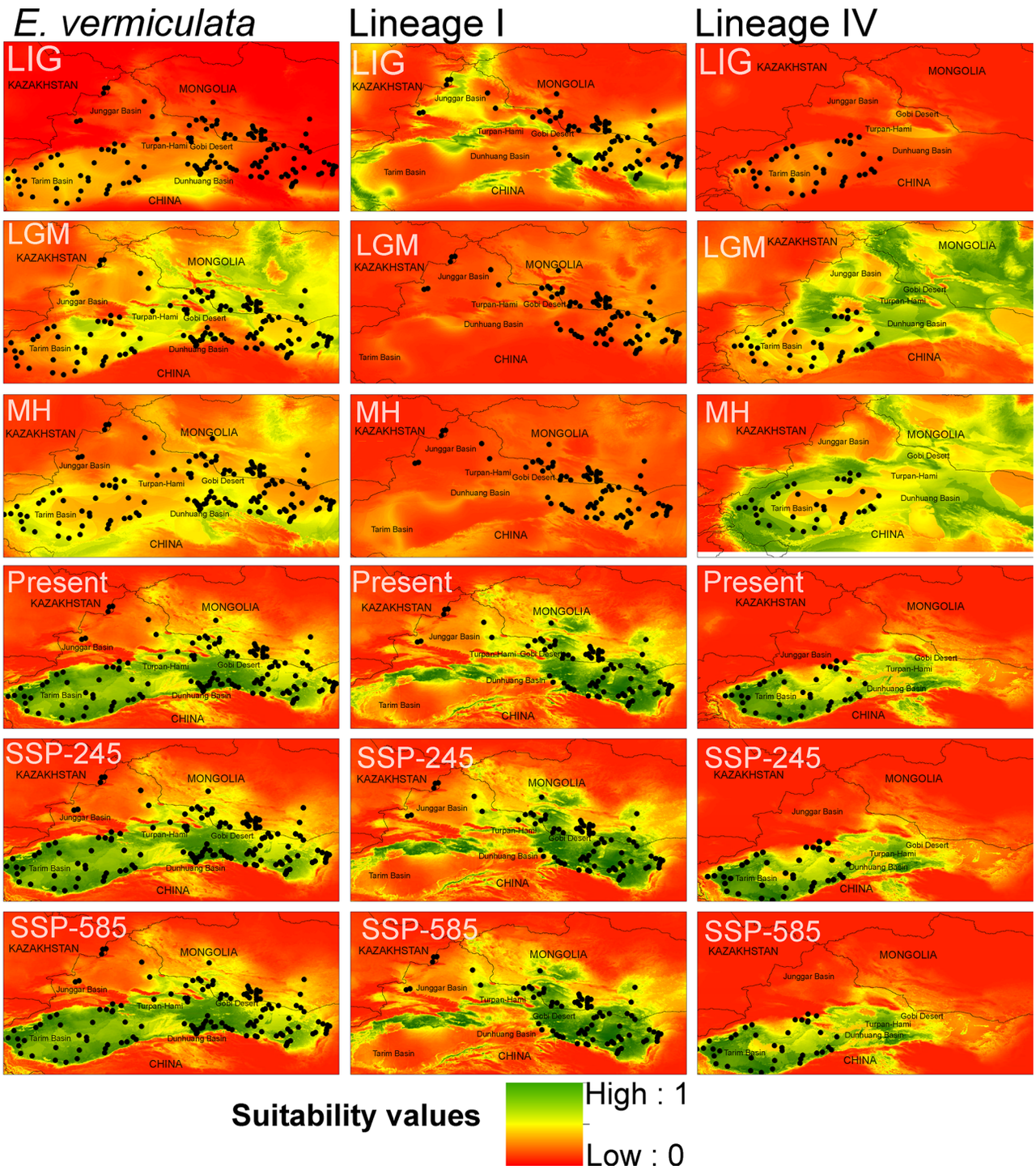


Figure 6 Potentially suitable distribution areas of *Eremias vermiculata* and intraspecific lineages estimated using the Maxent model across six time periods, including three paleoclimatic periods (Last Interglacial (LIG), Last Glacial Maximum (LGM), and mid-Holocene (MH)), present day, and two future climate scenarios (SSP245 and SSP585)

E. vermiculata: All populations of *E. vermiculata;* Lineage I: Population from the Mongolian Plateau; Lineage IV: Population from the Tarim and Yanqi Basins.

indistinguishable from random expectations under the equivalency framework. In contrast, niche similarity tests, which assess whether pairs of niches are more conserved than expected by chance, yielded divergent results. No significant niche conservatism was detected between Lineages I and III (P=0.059), failing to reject the null hypothesis of dissimilarity, whereas significant conservation was detected for I vs. IV (P=0.049) and III vs. IV (P=0.005) (Figure 8B), rejecting the null hypothesis of dissimilarity in both cases. These findings indicate that the niches of these lineage pairs exhibit greater similarity than expected by chance. The apparent discrepancy observed for Lineages III and IV—where niche equivalency was not supported (P=0.955), yet niche similarity was significant (P=0.005)—highlights the fundamentally different aims of the two tests: equivalency tests assess whether niches are

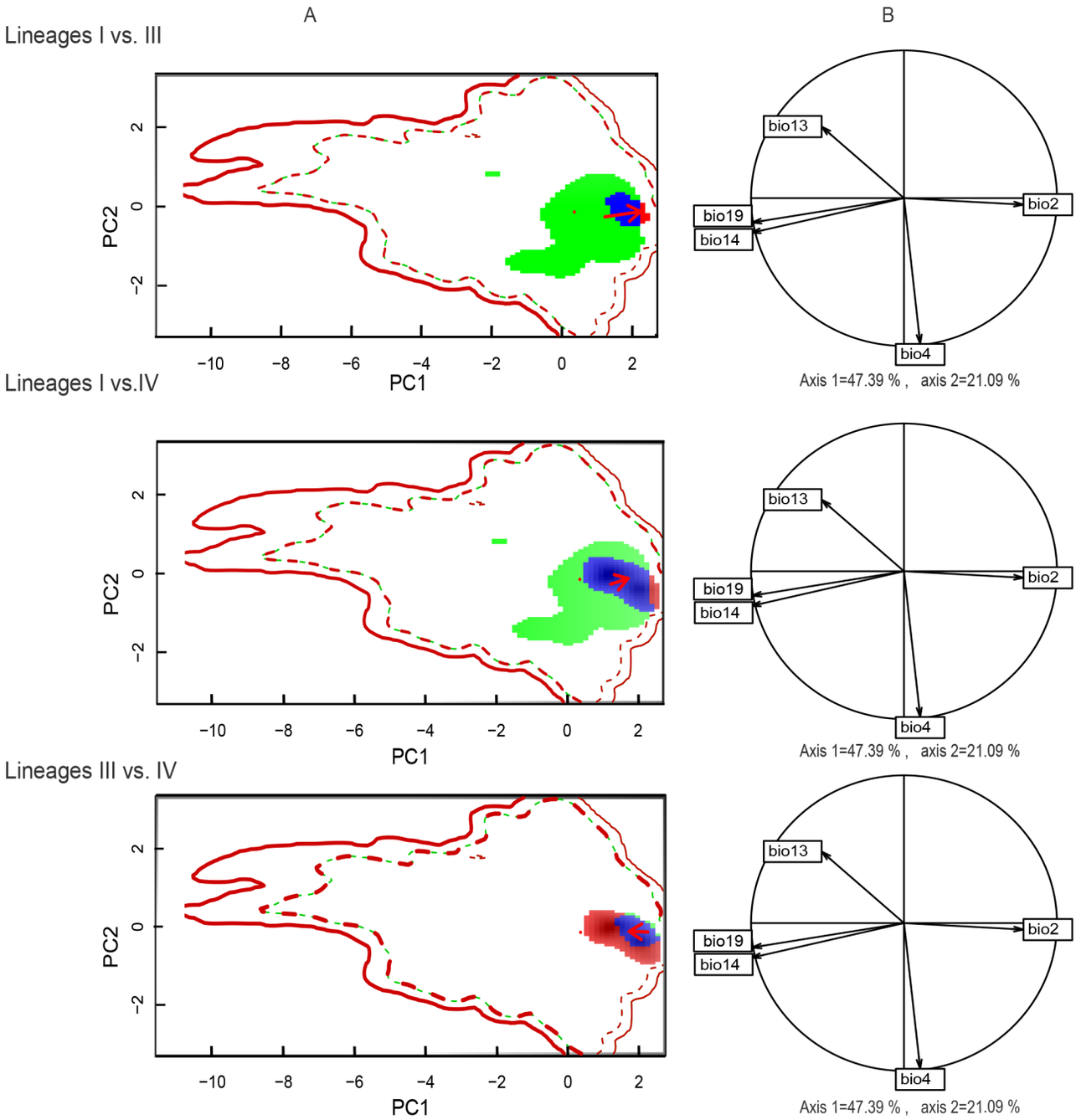


Figure 7 Principal component analysis of niche shifts among lineages

A: Green and red surfaces represent kernel densities as a function of the number of records from both lineages. Blue area is the overlap between these kernel estimates and reflects the magnitude of niche overlap between corresponding lineages. Red arrows indicate Schoener's *D* (niche overlap index) estimate. Solid and dashed contours represent 100% and 50% of the available environmental space, respectively. B: Orientation and relative contribution of variables within each quadrant of the principal component space.

statistically identical, whereas similarity tests evaluate whether niches are more conserved than expected given the environmental context of each lineage.

Collectively, these results suggest that while equivalency tests found no statistical evidence for niche divergence (all $P>0.05$), similarity tests revealed that some lineages (I-IV, III-IV) retained conserved ecological traits, likely shaped by shared evolutionary or environmental constraints.

DISCUSSION

Extensive geographic sampling across the AECA revealed pronounced spatial structuring of genetic variation in *E. vermiculata*, closely aligned with the topographic and desert dynamics of the region. This lizard species, typically confined to rugged terrain, sand dunes, and arid deserts at lower altitudes, exhibits limited dispersal capabilities, rendering it highly susceptible to landscape-induced genetic fragmentation. The impact of mountains on *E. vermiculata* dispersal is evident from the congruence between their genetic makeup and the geological features of the region. The genetic structure of *E. vermiculata* highlights the central role of landscape features and arid glaciation in shaping its genetic diversity.

Table 1 Schoener's *D* and Warren's *I* values indicate no niche overlap between lineages and values of expansion, stability, and unfilling, respectively

Values	*D* value	*I* value	Expansion	Stability	Unfilling
Lineages I vs. III	0.118	0.253	0.0831	0.9168	0.8874
Lineages I vs. IV	0.353	0.506	0.0728	0.9271	0.5028
Lineages III vs. IV	0.405	0.590	0.6381	0.3618	0.0296

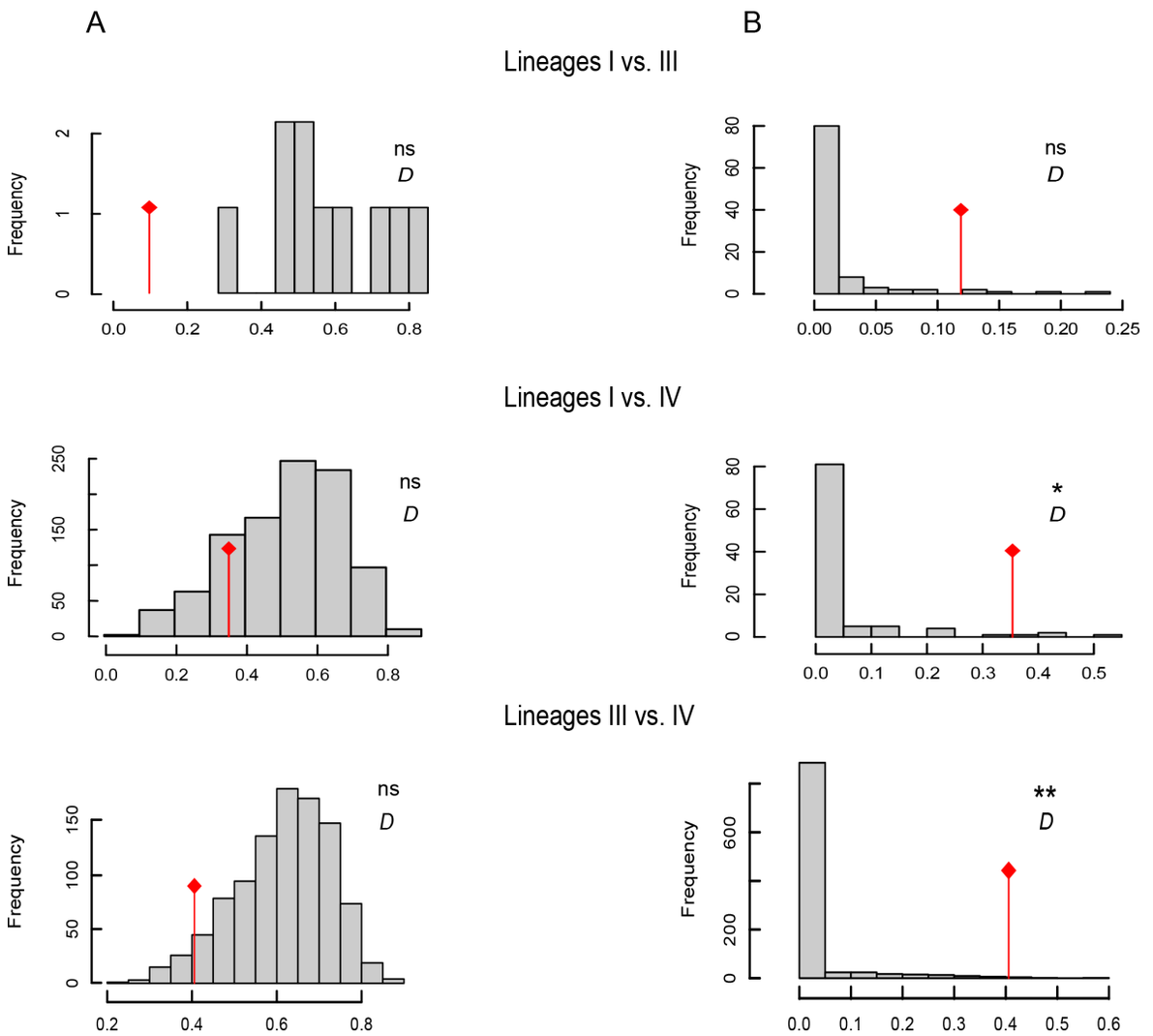


Figure 8 Niche comparisons among lineages under climatic ecological space

A: Histograms of niche equivalency tests between Lineages I, III, and IV. B: Niche similarity tests between Lineages I, III, and IV. Schoener's *D* index on the x-axis indicates no (*D*=0) to complete (*D*=1) niche overlap. Red vertical line represents observed value, while gray bars depict null distribution based on 1 000 random permutations. ns: Not significant; *: *P*<0.05; **: *P*<0.01.

Mito-nuclear discordance

The mito-nuclear discordance detected in *E. vermiculata* through haplotype network analysis suggests a rich and complex evolutionary history. mtDNA exhibited strong geographic structuring, with four major lineages (I, II, III, and IV) corresponding to distinct geographic regions (Figure 2B). In contrast, nuDNA revealed extensive haplotype sharing across geographically disparate regions, suggesting the persistence of ancestral polymorphisms. Notably, haplotypes from Lineages II and III were intermingled and also present in Lineage I, while Lineage III shared nuclear haplotypes with region IV (Figure 3), pointing to pronounced incongruence between mitochondrial and nuclear genomic patterns.

This discordance, a common phenomenon in many taxa, may arise from several evolutionary processes, such as incomplete lineage sorting (ILS), sex-biased dispersal, secondary contact, or introgressive hybridization (Toews & Brelsford, 2012). Among these, ILS represents the most parsimonious explanation for the observed patterns in *E. vermiculata*. This species occupies fragmented arid habitats below 2 000 m and exhibits limited dispersal ability, conditions that promote allopatric isolation and restrict gene flow. Given the larger effective population size and the slower coalescence of nuclear loci compared to mtDNA (Toews & Brelsford, 2012), the persistence of ancestral nuclear haplotypes across lineages is consistent with delayed lineage sorting. The shared haplotypes predominantly stemming from central rather than peripheral positions further supports the ILS hypothesis (Figure 3). Collectively, these patterns indicate that ILS may be the driving force behind the distinct mtDNA

pattern and shallow divergence observed in nuclear genes.

While alternative explanations, such as sex-biased dispersal, natural selection, hybridization, and secondary contact, cannot be entirely excluded, none are strongly supported by the available ecological or genetic evidence. In contrast, ILS driven by historical allopatric divergence offers a more consistent and compelling explanation for the observed mito-nuclear discordance in *E. vermiculata*. Nevertheless, further detailed studies are needed to fully understand this phenomenon within *E. vermiculata*. Such studies will be crucial for elucidating the complex interplay of evolutionary forces shaping the genetic architecture of this species. More broadly, elucidating the causes of mito-nuclear discordance in reptiles, given their unique characteristics, will provide valuable insights into their evolutionary trajectories, with important implications for conservation strategies and ecological research.

Genetic structure and its drivers

The topographic complexity within the AECA has exerted a pronounced effect on the genetic diversification of *E. vermiculata*. Phylogenetic analyses of mtDNA identified four geographically cohesive and genetically distinct lineages, each corresponding to a specific geographic region. Lineage I encompassed the Mongolian Plateau, including the Altai Gobi Desert, Alashan region, Hexi Corridor, Zaisan Depression, and Junggar Basin, while Lineage II was associated with the Turpan-Hami Basin, Lineage III was associated with the Dunhuang Basin, and Lineage IV included the Tarim and Yanqi Basins. The complete absence of shared haplotypes among these lineages underscores a strong phylogeographic signal shaped by geographic isolation.

Genetic divergence among lineages was further supported by pairwise uncorrected *p*-distances (0.014–0.048, mean of 0.036), with AMOVA results indicating that 84.65% of the genetic variation was partitioned among, rather than within, groups. Although MLPE modeling did not provide strong support for any single isolation model, the IBR model (e.g., elevation) showed the lowest AIC and BIC values (Supplementary Table S10), implicating mountain barriers in restricting gene flow. MRDM analyses provided further resolution, demonstrating that while both landscape resistance (IBR) and geographical distance (IBD) contributed to genetic differentiation in *E. vermiculata*, the latter exerted a stronger effect (Supplementary Table S10). In contrast, environmental factors (IBE) appeared to have a minimal effect on population differentiation in this species. Hydrographic features such as the Shule River may also influence genetic connectivity. Acting as a significant barrier, the river demarcates Lineage I in the Hexi Corridor from Lineage III in the Dunhuang Basin (Figure 1). The dynamic nature of the river, with a strong central current weakening towards its terminus, is likely to influence gene flow. In areas where the river is less formidable, genetic connectivity is possible, allowing for limited genetic exchange among populations. Despite the broad distribution of Lineage I, genetic homogeneity across this region implies relatively unrestricted gene flow. The Junggar Basin, encircled by mountains, remains somewhat isolated from adjacent desert habitats. Nevertheless, a narrow biogeographic corridor appears to facilitate connectivity between the basin and the Gobi region, supporting the maintenance of genetic similarity across these areas, as previously suggested by Xu et al. (2023). However, MJN analyses also revealed substructuring within Lineage I, indicating that fine-scale geographic isolation continues to shape regional differentiation.

Collectively, these findings highlight the primacy of geographical distance and topographic barriers in isolating lineages and populations. These results contrast with earlier work by Zhang et al. (2010) on a *P. axillaris* clade, which reported unrestricted gene flow between the Turpan-Hami and Tarim Basins and challenged the notion that geographic isolation necessarily leads to species differentiation. However, our findings, consistent with subsequent work on the same species (Li, 2013), support the view that each basin harbors evolutionarily distinct lineages of *E. vermiculata*, shaped by historical isolation and limited contemporary gene flow. This pattern emphasizes the importance of historical vicariance, orographic barriers, and climatic change in structuring population divergence and potentially speciation. These findings contribute to a broader understanding of how geography and climatic events have shaped the genetic diversity and distribution patterns of *E. vermiculata* and provide a basis for further studies of the evolutionary history and biogeography of the species.

Temporal and spatial evolution of *E. vermiculata*

Molecular dating estimated the intraspecific diversification of *E. vermiculata* at around 1.18 Ma, aligning with a period of intensified tectonic activity and climatic shifts across inland Asia (Figure 4). Species divergence appears to have been shaped by uplift of the Tianshan and Altai mountain ranges and episodic aridification, which influenced the distribution and ecological adaptations of the species.

The accelerated uplift of the Tianshan and Altai mountain ranges between 2 and 3 Ma (Buslov et al., 2008), coupled with the rapid uplift of the Kunlun Mountains and Qinghai-Xizang Plateau during the Pleistocene (Fu et al., 2024), likely imposed significant topographic barriers that restricted gene flow and promoted divergence of the species within the region. Simultaneously, stepwise intensification of aridity in inland Asia around 2.6 Ma and 0.9 Ma (Sun et al., 2010) facilitated the formation of deserts, such as the Badain Jaran, Tengger, Gurbantunggut, and Mu Us deserts, which likely provided and refined the habitat of *E. vermiculata*, as noted by Li et al. (2018), Wang et al. (2015), and Zhao et al. (2022).

The Xixiabangma glaciation period (1.17–0.8 Ma), characterized by colder and more extreme conditions than the LGM (Li et al., 2018; Wang et al., 2015; Zhao et al., 2022; Zhou et al., 2006), may have further shaped the evolutionary trajectory of *E. vermiculata*. The species occupies cold desert habitats and is frequently found in open, arid landscapes with sandy or rocky substrates and dune systems (Editorial Committee of Zoology of China, Chinese Academy of Sciences, 1999). These habitat preferences suggest that glacial-period conditions may have favored ecological expansion and niche specialization. The emergence of fragmented dune ecosystems, coupled with the formation of montane barriers, likely facilitated lineage isolation and divergence. Together, these geological and climatic processes appear to have driven the spatial structuring, ecological differentiation, and diversification of *E. vermiculata* across the AECA.

Divergence among *E. vermiculata* lineages, particularly the split between Lineages I and II (~0.47 Ma) and Lineages III and IV (~0.45 Ma), showed close correspondence with major

geological and climatic shifts in the study area. During the Middle Pleistocene, the ancient Lop Nor paleolake extended westward toward Yumen Pass in the Dunhuang National Yadan Geopark. Approximately 0.3 Ma, substantial uplift of the Tibetan Plateau altered atmospheric circulation by obstructing the incursion of moist air masses, thereby intensifying regional aridification and establishing the present environmental patterns (Qu et al., 2004). Concurrently, the tectonic uplift of the Beishan Mountains likely acted as a natural barrier for *E. vermiculata*, a species more adapted to lower altitudes, effectively isolating the Alashan Plateau population (Lineage I) from the Turpan-Hami Basin population (Lineage II), with a divergence time of 0.47 Ma.

The divergence time of approximately 0.45 Ma (95% HPD: 0.05–0.75 Ma) for Lineage III (Dunhuang Basin) and Lineage IV (Tarim Basin) is also consistent with this period of intense landscape reconfiguration. The potential northward expansion of the Kumtag Desert, proposed by Qu et al. (2004), may have further contributed to habitat fragmentation. While it remains uncertain whether *E. vermiculata* tracked this desert expansion, the coincident timing suggests that these geomorphological dynamics may have contributed to lineage diversification. Similar patterns of divergence linked to Middle Pleistocene environmental transitions have been reported for other taxa in the region (Xu et al., 2023; Zhang et al., 2013), reinforcing the notion that paleogeographic events have played a central role in shaping reptilian diversification across the AECA (Liu et al., 2019; Wu et al., 2023). A key finding of this study is the identification of pronounced genetic divergence within the Tarim Basin, supporting the hypothesis of paleolake influence on demographic patterns. Network analysis of Lineage IV revealed two subgroups—western and eastern—indicating spatial subdivision within the basin (Supplementary Figure S2). While some haplotypes are centrally shared between these substructures, suggesting historical gene flow, the presence of more recent haplotypes in the western group suggests limited current gene flow from east to west. This pattern was confirmed by AMOVA, which attributed approximately 50% of the observed genetic variance to differences between the two groups (Supplementary Table S9).

The complex topography and historical elements of the Tarim Basin appear to have significantly influenced species distribution. The western basin is dominated by sandy deserts with expansive dune fields, exemplified by the Taklamakan Desert. In contrast, the eastern Basin features a more diverse landscape, including deserts, oases, and isolated mountain ranges, as observed during our fieldwork. These contrasting environments likely provided varying selective pressures and dispersal constraints, shaping lineage divergence. Moreover, the historical presence of a large lake in the center of the Tarim Basin around 40 000 to 30 000 years ago (Yang et al., 2011; Yang & Scuderi, 2010) may have further influenced population distributions, forcing taxa toward peripheral habitats. This scenario is consistent with the proposed paleolake hypothesis used to explain the distribution of *P. axillaris* (Li, 2013), but contrasts with alternative interpretations linking *P. axillaris* population structure primarily to river systems and modern oases (Zhang et al., 2010). Collectively, our findings support the existence of a paleolake, indicating a dynamic and changing topography that has shaped the genetic landscape of the region.

Lineage-specific population expansion during arid glacial periods

Our genetic and ecological evidence indicated that all *E. vermiculata* lineages underwent a demographic expansion during the Late Pleistocene, coinciding with arid glacial intervals. This expansion appears to have been facilitated by the absence of extensive glaciation, the expansion of arid habitats, and the intensification of desertification during the LGM, which collectively created favorable conditions for population growth and westward migration.

These findings are strongly supported by the strongly negative Tajima's *D* and Fu's *Fs*, low R_2 tests, unimodal mismatch distributions, and Bayesian skyline plots (Supplementary Table S8 and Figure 5). Furthermore, ENM based on species-wide occurrence records (Figure 6A) revealed spatial expansion during the LGM, with climatically suitable habitats concentrated in the northern and southeastern regions of the Gobi Desert, Mongolian Plateau, and Turpan-Hami Basin. This congruence between ecological and genetic data suggests that *E. vermiculata* was minimally affected by glacial maxima in these regions. The resilience of this species is consistent with the topographic characteristics of these areas, particularly the Gobi Desert, which has been documented to be largely unaffected by Quaternary climate fluctuations due to its southern temperate montane climate (Sakka et al., 2010). Consequently, these areas may have served as glacial refugia, enabling population persistence and expansion during severe climatic phases. It is therefore reasonable to infer that the effective population size of *E. vermiculata* would likely have increased during glacial periods, further shaping its demographic history and current genetic diversity.

Lineage-specific demographic reconstructions further revealed distinct patterns of expansion and contraction. BSP analyses demonstrated a marked population increase in Lineage I around 10 000 years ago, a signal strongly supported by significantly negative Tajima's *D* (−2.683) and Fu's *Fs* (−26.395) and a low R_2 value (0.007), consistent with recent demographic growth. In contrast, Lineage IV exhibited a pronounced expansion approximately 5 000 years ago, followed by a recent contraction. Despite overall demographic stability during the LGM, the observed negative neutrality statistics and low R_2 values across several lineages (Supplementary Table S8 and Figure 5) provide additional evidence for recent population expansions. These temporal demographic patterns are congruent with the ENM results. For Lineage IV, ENM results showed a broader potential distribution during the LGM and mid-Holocene compared to present day (Figure 6C). This historical expansion and subsequent contraction highlight the dynamic nature of population fluctuations in response to climatic and environmental changes over time. The consistency between the genetic and ecological findings highlights the importance of considering both historical and contemporary factors when assessing the demographic history of species. Such comprehensive analyses provide valuable insights into the complex interplay among geological events, climatic shifts, genetic diversity, and species distribution.

The marked expansion of *E. vermiculata* during the LGM is consistent with its adaptation to cold-arid environments and reflects broader ecological dynamics within Central Asia. Several converging factors likely contributed to its survival and expansion: (i) Glacial exclusion: the western Gobi Desert, a

core part of the species' range, remained free of glacial coverage during the LGM (Shi et al., 2009), providing a stable climatic refugium; (ii) Expansion of arid habitats: the substantial increase in arid habitats during the LGM (Lu et al., 2019) led to the widespread proliferation of sand dunes, rocky terrain, and steppe deserts, which constitute suitable habitats for the species; (iii) Desert expansion: the continued expansion of the Taklamakan Desert during the mid-Pleistocene increased the aridity and temperature extremes across the eastern Tianshan, Turpan-Hami Basin, and lower Hexi Corridor (Wang et al., 2016; Wu, 1981), creating suitable habitats, including burrows, that allowed the species to thrive and adapt to more extreme conditions; (iv) Palaeohydrological regression: the disappearance of Pleistocene lakes in the Turpan Depression and concurrent desertification during the Late Pleistocene (Bubenzer et al., 2016; Lu et al., 2013; Yang et al., 2011) may have driven population shifts toward the northwestern areas of the range. Consistent with this trajectory, ENMs of mid-Holocene distribution indicated that Lineage IV expanded into the western Tarim Basin (Figure 6C), likely facilitated by ongoing climatic aridification that promoted the establishment of arid-adapted assemblages.

The demographic stability of *E. vermiculata* during the LGM aligns with patterns observed in other cold-arid-adapted taxa across the region. For instance, the arid-adapted scorpion *Mesobuthus mongolicus* experienced exponential growth during the LGM, a period when global ice sheets and mountain glaciers were at their greatest extent, between approximately 26 500 and 19 000 years ago (Clark et al., 2009). The closely related species *E. roborowskii* maintained a stable population over the same period (Liu et al., 2019). Similar expansion patterns have been documented in other desert-dwelling vertebrates, including gerbils (Wang et al., 2013), hamsters (Lv et al., 2016), toad-headed lizards (Wu et al., 2023), and various desert plants inhabiting the Gobi region (Meng & Zhang, 2013; Shi & Zhang, 2015). These findings, corroborated by genetic and phylogeographic data, support the hypothesis of range expansion for cold-arid-adapted species during the LGM (Galbreath et al., 2009; Kearns et al., 2014).

CONCLUSIONS

Our comprehensive study, covering different geographical areas of the AECA region, supports the use of *E. vermiculata* as a model for understanding AECA biogeography and the impact of geological and climatic history on genetic diversity and demography. Integrative analyses identified significant mito-nuclear discordance in *E. vermiculata*, suggesting complex evolutionary dynamics. Furthermore, the genetic structure of this species closely followed the topography of the AECA, suggesting that geographic barriers have played a key role in shaping population differentiation. Notably, the strong genetic divergence within the Tarim Basin, together with signals of population expansion, supports the hypothesis that both paleolake dynamics and glacial cycles shaped the demographic history of *E. vermiculata*. The strong correlation between the genetic patterns of *E. vermiculata* and the AECA landscape highlights the importance of reptiles as model organisms for studying phylogeographic patterns in arid regions of Central Asia. Overall, this study demonstrates that environmental dynamism has played a critical role in shaping species distribution and lineage divergence, and emphasizes the importance of adaptive management strategies to mitigate the impacts of ongoing and future environmental change on biodiversity.

SCIENTIFIC FIELD SURVEY PERMISSION INFORMATION

Permission for field surveys was granted by the Forestry Department and National Reserves of China and the Committee for Forestry and Hunting of the Ministry of Environmental Protection of Kazakhstan.

DATA AVAILABILITY

All novel sequences were deposited at the Science Data Bank (https://cstr.cn/31253.11.sciencedb.21707). A full list of the NCBI GenBank accession numbers is available in Supplementary Table S1.

SUPPLEMENTARY DATA

Supplementary data to this article can be found online.

COMPETING INTERESTS

The authors declare that they have no competing interests.

AUTHORS' CONTRIBUTIONS

A.A.: Methodology, Investigation, Formal analysis, Visualization, Validation, Writing – original draft, Writing – review & editing. D.L.C.: Investigation, Formal analysis, Funding acquisition, Writing – review & editing. T.N.D.: Resources, Validation, Writing – review & editing. Q.S.: Investigation, Writing – review & editing. K.T.: Resources, Writing – review & editing. J.L.: Resources, Writing – review & editing. Y.Q.: Resources, Writing – review & editing. X.G.G.: Conceptualization, Methodology, Investigation, Resources, Visualization, Validation, Supervision, Funding acquisition, Project administration, Writing – review & editing. All authors read and approved the final version of the manuscript.

ACKNOWLEDGMENTS

We would like to thank members of staff at the Chengdu Institute of Biology, Chinese Academy of Sciences, including Jin-Long Liu, Tian-He Zhou, Yue-Zhao Wang, Qiang Dai, Bo Cai, Yong Huang, Xiong Gong, Da-Jiang Li, and Min-Li Chen, as well as Marina Chirikova from the Institute of Zoology, Ministry of Science and Higher Education of the Republic of Kazakhstan, for their help with sample collection. We thank Jinzhong Fu (University of Guelph) for providing tissue samples under his care. We thank Yong-Fei He for kind help during field work. We are especially grateful to Tian-He Zhou, Rui Xu, and Zi-Hui Cai (Chengdu Institute of Biology, Chinese Academy of Sciences) for their help in the laboratory. We would also like to thank Pedro Tarroso and an anonymous referee for their insightful comments and suggestions on the manuscript.

REFERENCES

Ackerly DD, Loarie SR, Cornwell WK, et al. 2010. The geography of climate change: implications for conservation biogeography. *Diversity and Distribution*, **16**(3): 476–487.

Anadón JD, Graciá E, Botella F, et al. 2015. Individualistic response to past climate changes: niche differentiation promotes diverging quaternary range dynamics in the subspecies of *Testudo graeca*. *Ecography*, **38**(9): 956–966.

Austin AT. 2011. Has water limited our imagination for aridland biogeochemistry? *Trends in Ecology & Evolution*, **26**(5): 229–235.

Avise JC. 2000. Phylogeography: The History and Formation of Species. Cambridge: Harvard University Press, 447.

Avise JC. 2009. Phylogeography: retrospect and prospect. *Journal of Biogeography*, **36**(1): 3–15.

Avise JC, Bowen BW, Ayala FJ. 2016. In the light of evolution X: comparative phylogeography. *Proceedings of the National Academy of Sciences of the United States of America*, **113**(29): 7957–7961.

Bandelt HJ, Forster P, Röhl A. 1999. Median-joining networks for inferring

intraspecific phylogenies. *Molecular Biology and Evolution*, **16**(1): 37–48.
Barbolini N, Woutersen A, Dupont-Nivet G, et al. 2020. Cenozoic evolution of the steppe-desert biome in Central Asia. *Science Advances*, **6**(41): eabb8227.
Brandley MC, Guiher TJ, Pyron RA, et al. 2010. Does dispersal across an aquatic geographic barrier obscure phylogeographic structure in the diamond-backed watersnake (*Nerodia rhombifer*)?. *Molecular Phylogenetics and Evolution*, **57**(2): 552–560.
Broennimann O, Fitzpatrick MC, Pearman PB, et al. 2012. Measuring ecological niche overlap from occurrence and spatial environmental data. *Global Ecology and Biogeography*, **21**(4): 481–497.
Brown JL, Bennett JR, French CM. 2017. SDMtoolbox 2.0: the next generation Python-based GIS toolkit for landscape genetic, biogeographic and species distribution model analyses. *PeerJ*, **5**: e4095.
Bubenzer O, Hecht S, Li CS, et al. 2016. Late Pleistocene (MIS2) environmental changes and palaeoclimatic dynamics around Aiding Lake in the Turpan Basin, Xinjiang province, NW-China. *Zeitschrift für Geomorphologie*, **60**(S1): 5–27.
Buslov MM, Kokh DA, De Grave J. 2008. Mesozoic-Cenozoic tectonics and geodynamics of Altai, Tien Shan, and Northern Kazakhstan, from apatite fission-track data. *Russian Geology and Geophysics*, **49**(9): 648–654.
Byrne M, Joseph L, Yeates DK, et al. 2018. Evolutionary history. *In*: Lambers H. On the Ecology of Australia's Arid Zone. Cham: Springer, 45–75.
Byrne M, Yeates DK, Joseph L, et al. 2008. Birth of a biome: insights into the assembly and maintenance of the Australian arid zone biota. *Molecular Ecology*, **17**(20): 4398–4417.
Chang CW, Fridman E, Mascher M, et al. 2022. Physical geography, isolation by distance and environmental variables shape genomic variation of wild barley (*Hordeum vulgare* L. ssp. *spontaneum*) in the Southern Levant. *Heredity*, **128**(2): 107–119.
Chen DL, Su XL, Liu JL, et al. 2019. Next-generation sequencing yields a nearly complete mitochondrial genome of the variegated racerunner (*Eremias vermiculata*) from Dunhuang Basin. *Mitochondrial DNA Part B*, **4**(1): 1626–1627.
Chen X, Jiang FQ, Wang YJ, et al. 2013. Characteristics of the eco-geographical pattern in arid land of Central Asia. *Arid Zone Research*, **30**(3): 385–390. (in Chinese)
Clark PU, Dyke AS, Shakun JD, et al. 2009. The last glacial maximum. *Science*, **325**(5941): 710–714.
Clarke RT, Rothery P, Raybould AF. 2002. Confidence limits for regression relationships between distance matrices: estimating gene flow with distance. *Journal of Agricultural, Biological, and Environmental Statistics*, **7**(3): 361–372.
Davis MB, Shaw RG, 2001. Range shifts and adaptive responses to Quaternary climate change. *Science*, **292**(5517): 673–679.
Di Cola V, Broennimann O, Petitpierre B, et al. 2017. ecospat: an R package to support spatial analyses and modeling of species niches and distributions. *Ecography*, **40**(6): 774–787.
Dixon P. 2003. VEGAN, a package of R functions for community ecology. *Journal of Vegetation Science*, **14**(6): 927–930.
Drummond AJ, Suchard MA, Xie D, et al. 2012. Bayesian phylogenetics with BEAUti and the BEAST 1.7. *Molecular Biology and Evolution*, **29**(8): 1969–1973.
Editorial Committee of Zoology of China, Chinese Academy of Sciences. 1999. Fauna Sinica, Reptilia, Vol. 2, Squamata, Lacertilia. Beijing: Science Press, 394. (in Chinese)
Ersts PJ. 2024(2024-08-29). Geographic distance matrix generator (version 1.2. 3). American Museum of Natural History. http://biodiversityinformatics.amnh.org/open_source/gdmg.
Excoffier L, Lischer HEL. 2010. Arlequin suite ver 3.5: a new series of programs to perform population genetics analyses under Linux and Windows. *Molecular Ecology Resources*, **10**(3): 564–567.
Fang XM, An ZS, Clemens SC, et al. 2020. The 3.6-Ma aridity and westerlies history over midlatitude Asia linked with global climatic cooling. *Proceedings of the National Academy of Sciences of the United States of America*, **117**(40): 24729–24734.
Fick SE, Hijmans RJ. 2017. WorldClim 2: new 1-km spatial resolution climate surfaces for global land areas. *International Journal of Climatology*, **37**(12): 4302–4315.
Fu RR, Zhu YX, Liu Y, et al. 2024. Shared xerophytic genes and their re‐use in local adaptation to aridity in the desert plant *Gymnocarpos przewalskii*. *Molecular Ecology*, **33**(12): e17380.
Fu YX. 1997. Statistical tests of neutrality of mutations against population growth, hitchhiking and background selection. *Genetics*, **147**(2): 915–925.
Galbreath KE, Hafner DJ, Zamudio KR. 2009. When cold is better: climate-driven elevation shifts yield complex patterns of diversification and demography in an alpine specialist (American Pika, *Ochotona princeps*). *Evolution*, **63**(11): 2848–2863.
Garcia RA, Cabeza M, Rahbek C, et al. 2014. Multiple dimensions of climate change and their implications for biodiversity. *Science*, **344**(6183): 1247579.
Goslee SC, Urban DL. 2007. The ecodist package for dissimilarity-based analysis of ecological data. *Journal of Statistical Software*, **22**(7): 1–19.
Gouy M, Guindon S, Gascuel O. 2010. SeaView version 4: a multiplatform graphical user interface for sequence alignment and phylogenetic tree building. *Molecular Biology and Evolution*, **27**(2): 221–224.
Guo XG, Dai X, Chen DL, et al. 2011. Phylogeny and divergence times of some racerunner lizards (Lacertidae: *Eremias*) inferred from mitochondrial 16S rRNA gene segments. *Molecular Phylogenetics and Evolution*, **61**(12): 400–412.
Harpending HC. 1994. Signature of ancient population growth in a low-resolution mitochondrial DNA mismatch distribution. *Human Biology*, **66**(4): 591–600.
Hewitt G. 2000. The genetic legacy of the Quaternary ice ages. *Nature*, **405**(6789): 907–913.
Hewitt GM. 2004. Genetic consequences of climatic oscillations in the Quaternary. *Philosophical Transactions of the Royal Society B: Biological Sciences*, **359**(1442): 183–195.
Hickerson MJ, Carstens BC, Cavender-Bares J, et al. 2010. Phylogeography's past, present, and future: 10 years after Avise, 2000. *Molecular Phylogenetics and Evolution*, **54**(1): 291–301.
Hijmans RJ, Cameron SE, Parra JL, et al. 2005. Very high resolution interpolated climate surfaces for global land areas. *International Journal of Climatology*, **25**(15): 1965–1978.
Jiao XL, Wu L, Zhang DZ, et al. 2024. Landscape heterogeneity explains the genetic differentiation of a forest bird across the Sino-Himalayan Mountains. *Molecular Biology and Evolution*, **41**(3): msae027.
Kass RE, Raftery AE. 1995. Bayes factors. *Journal of the American Statistical Association*, **90**(430): 773–795.
Kearns AM, Joseph L, Toon A, et al. 2014. Australia's arid-adapted butcherbirds experienced range expansions during Pleistocene glacial maxima. *Nature Communications*, **5**: 3994.
Keppel G, van Niel KP, Wardell-Johnson GW, et al. 2012. Refugia: identifying and understanding safe havens for biodiversity under climate change. *Global Ecology and Biogeography*, **21**(4): 393–404.
Lanfear R, Frandsen PB, Wright AM, et al. 2017. PartitionFinder 2: new methods for selecting partitioned models of evolution for molecular and morphological phylogenetic analyses. *Molecular Biology and Evolution*, **34**(3): 772–773.
Li J. 2013. The Characteristics of Mitochondrial Genome of the Yarkand Toad-Headed Agama and Its Phylogeography Inferred from ND4-tRN^{Leu}

Gene Segments. Ph. D. dissertation, University of Chinese Academy of Sciences, Beijing. (in Chinese)

Li ZJ, Wang F, Wang X, et al. 2018. A multi-proxy climatic record from the central Tengger Desert, southern Mongolian Plateau: implications for the aridification of inner Asia since the late Pliocene. *Journal of Asian Earth Sciences*, **160**: 27–37.

Liu JL, Guo XG, Chen DL, et al. 2019. Diversification and historical demography of the rapid racerunner (*Eremias velox*) in relation to geological history and Pleistocene climatic oscillations in arid Central Asia. *Molecular Phylogenetics and Evolution*, **130**: 244–258.

Liu JL, Yuan XY, Zhou TH, et al. 2014. *Eremias vermiculata* was discovered in the North of Tianshan Mountains in Xinjiang Uygur Autonomous Region. *Chinese Journal of Zoology*, **49**(3): 423–427. (in Chinese)

Liu WG, Liu ZH, Sun JM, et al. 2020. Onset of permanent Taklimakan Desert linked to the mid-Pleistocene transition. *Geology*, **48**(8): 782–786.

Lu HY, Wang XY, Wang XY, et al. 2019. Formation and evolution of Gobi Desert in central and eastern Asia. *Earth-Science Reviews*, **194**: 251–263.

Lu HY, Yi SW, Xu ZW, et al. 2013. Chinese deserts and sand fields in Last Glacial Maximum and Holocene Optimum. *Chinese Science Bulletin*, **58**(23): 2775–2783.

Lv X, Xia L, Ge DY, et al. 2016. Continental refugium in the Mongolian Plateau during Quaternary glacial oscillations: phylogeography and niche modelling of the endemic desert hamster, *Phodopus roborovskii*. *PLoS One*, **11**(2): e0148182.

Maestre FT, Benito BM, Berdugo M, et al. 2021. Biogeography of global drylands. *New Phytologist*, **231**(2): 540–558.

McRae BH. 2006. Isolation by resistance. *Evolution*, **60**(8): 1551–1561.

McRae BH, Dickson BG, Keitt TH, et al. 2008. Using circuit theory to model connectivity in ecology, evolution, and conservation. *Ecology*, **89**(10): 2712–2724.

Melville J, Hale J, Mantziou G, et al. 2009. Historical biogeography, phylogenetic relationships and intraspecific diversity of agamid lizards in the Central Asian deserts of Kazakhstan and Uzbekistan. *Molecular Phylogenetics and Evolution*, **53**(1): 99–112.

Meng HH, Zhang ML. 2013. Diversification of plant species in arid Northwest China: species-level phylogeographical history of *Lagochilus* Bunge ex Bentham (Lamiaceae). *Molecular Phylogenetics and Evolution*, **68**(3): 398–409.

Minh BQ, Nguyen MAT, von Haeseler A. 2013. Ultrafast approximation for phylogenetic bootstrap. *Molecular Biology and Evolution*, **30**(5): 1188–1195.

Naimi B, Araújo MB. 2016. sdm: a reproducible and extensible R platform for species distribution modelling. *Ecography*, **39**(4): 368–375.

Naimi B, Hamm NAS, Groen TA, et al. 2014. Where is positional uncertainty a problem for species distribution modelling?. *Ecography*, **37**(2): 191–203.

Newton MA, Raftery AE. 1994. Approximate Bayesian inference with the weighted likelihood bootstrap. *Journal of the Royal Statistical Society: Series B (Methodological)*, **56**(1): 3–48.

Nguyen LT, Schmidt HA, von Haeseler A, et al. 2015. IQ-TREE: a fast and effective stochastic algorithm for estimating maximum-likelihood phylogenies. *Molecular Biology and Evolution*, **32**(1): 268–274.

Pavlicev M, Mayer W. 2009. Fast radiation of the subfamily Lacertinae (Reptilia: Lacertidae): History or methodical artefact?. *Molecular Phylogenetics and Evolution*, **52**(3): 727–734.

Pearman PB, D'Amen M, Graham CH, et al. 2010. Within‐taxon niche structure: niche conservatism, divergence and predicted effects of climate change. *Ecography*, **33**(6): 990–1003.

Pepper M, Keogh JS. 2021. Life in the "dead heart" of Australia: the geohistory of the Australian deserts and its impact on genetic diversity of arid zone lizards. *Journal of Biogeography*, **48**(4): 716–746.

Peterman WE. 2018. ResistanceGA: an R package for the optimization of resistance surfaces using genetic algorithms. *Methods in Ecology and Evolution*, **9**(6): 1638–1647.

Peterson AT, Soberón J, Sánchez-Cordero V. 1999. Conservatism of ecological niches in evolutionary time. *Science*, **285**(5431): 1265–1267.

Phillips SJ, Anderson RP, Schapire RE. 2006. Maximum entropy modeling of species geographic distributions. *Ecological Modelling*, **190**(3-4): 231–259.

Qiao HJ, Peterson AT, Ji LQ, et al. 2017. Using data from related species to overcome spatial sampling bias and associated limitations in ecological niche modelling. *Methods in Ecology and Evolution*, **8**(12): 1804–1812.

Qu JJ, Zheng BX, Yu QH, et al. 2004. The Yardang landform of Aqik Valley in the east of Lop-Nor and its relationship with the evolution of the Kumtagh Desert. *Journal of Desert Research*, **24**(3): 294–300. (in Chinese)

Rambaut A. 2016. Figtree 1.4. 4. Computer program and documentation distributed by the author. https://github.com/rambaut/figtree/releases/tag/v1.4.4.

Rambaut A, Drummond AJ. 2007. Tracer v1.4. Computer program and documentation distributed by the author. http://beast.bio.ed.ac.uk/Tracer.

Rambaut A, Drummond AJ, Xie D, et al. 2018. Posterior summarization in Bayesian phylogenetics using Tracer 1.7. *Systematic Biology*, **67**(5): 901–904.

Ramos-Onsins SE, Rozas J. 2002. Statistical properties of new neutrality tests against population growth. *Molecular Biology and Evolution*, **19**(12): 2092–2100.

Revelle W. 2017(2017-01-07). Using the psych package to generate and test structural models. https://personality-project.org/r/psych_for_sem.pdf.

Reynolds JF, Smith DMS, Lambin EF, et al. 2007. Global desertification: building a science for dryland development. *Science*, **316**(5826): 847–851.

Ritchie AM, Lo N, Ho SYW. 2017. The impact of the tree prior on molecular dating of data sets containing a mixture of inter-and intraspecies sampling. *Systematic Biology*, **66**(3): 413–425.

Ronquist F, Teslenko M, van Der Mark P, et al. 2012. MrBayes 3.2: efficient Bayesian phylogenetic inference and model choice across a large model space. *Systematic Biology*, **61**(3): 539–542.

Rozas J, Ferrer-Mata A, Sánchez-DelBarrio JC, et al. 2017. DnaSP 6: DNA sequence polymorphism analysis of large data sets. *Molecular Biology and Evolution*, **34**(12): 3299–3302.

Sakka H, Quéré JP, Kartavtseva I, et al. 2010. Comparative phylogeography of four *Apodemus* species (Mammalia: Rodentia) in the Asian Far East: evidence of Quaternary climatic changes in their genetic structure. *Biological Journal of the Linnean Society*, **100**(4): 797–821.

Schimel DS. 2010. Drylands in the earth system: a study of one of the world's driest forests elucidates the climatic effects of drylands. *Science*, **327**(5964): 418–419.

Serra-Varela MJ, Grivet D, Vincenot L, et al. 2015. Does phylogeographical structure relate to climatic niche divergence? A test using maritime pine (*Pinus pinaster* Ait.). *Global Ecology and Biogeography*, **24**(11): 1302–1313.

Shi CM, Zhang XS, Liu L, et al. 2023. Phylogeography of the desert scorpion illuminates a route out of Central Asia. *Current Zoology*, **69**(4): 442–455.

Shi XJ, Zhang ML. 2015. Phylogeographical structure inferred from cpDNA sequence variation of *Zygophyllum xanthoxylon* across north-west China. *Journal of Plant Research*, **128**(2): 269–282.

Shi YF, Liu CH, Kang ES. 2009. The glacier inventory of China. *Annals of Glaciology*, **50**(53): 1–4.

Smith AB, Godsoe W, Rodríguez-Sánchez F, et al. 2019. Niche estimation above and below the species level. *Trends in Ecology & Evolution*, **34**(3): 260–273.

Stephens M, Donnelly P. 2003. A comparison of Bayesian methods for haplotype reconstruction from population genotype data. *American Journal of Human Genetics*, **73**(5): 1162–1169.

Stephens M, Smith NJ, Donnelly P. 2001. A new statistical method for haplotype reconstruction from population data. *American Journal of Human Genetics*, **68**(4): 978–989.

Stewart JR, Lister AM, Barnes I, et al. 2010. Refugia revisited: individualistic responses of species in space and time. *Proceedings of the Royal Society B: Biological Sciences*, **277**(1682): 661–671.

Suchard MA, Lemey P, Baele G, et al. 2018. Bayesian phylogenetic and phylodynamic data integration using BEAST 1.10. *Virus Evolution*, **4**(1): vey016.

Sun JM, Ye J, Wu WY, et al. 2010. Late Oligocene–Miocene mid-latitude aridification and wind patterns in the Asian interior. *Geology*, **38**(6): 515–518.

Szczerbak NN. 2003. Guide to the Reptiles of the Eastern Palearctic. Malabar: Krieger Publishing Company, 260.

Tajima F. 1989. Statistical method for testing the neutral mutation hypothesis by DNA polymorphism. *Genetics*, **123**(3): 585–595.

Tamar K, Carranza S, Sindaco R, et al. 2016. Out of Africa: phylogeny and biogeography of the widespread genus *Acanthodactylus* (Reptilia: Lacertidae). *Molecular Phylogenetics and Evolution*, **103**: 6–18.

Tamura K, Stecher G, Kumar S. 2021. MEGA11: molecular evolutionary genetics analysis version 11. *Molecular Biology and Evolution*, **38**(7): 3022–3027.

Toews DPL, Brelsford A. 2012. The biogeography of mitochondrial and nuclear discordance in animals. *Molecular Ecology*, **21**(16): 3907–3930.

Tong QL, Yao YT, Lin LH, et al. 2016. The complete mitochondrial genome of *Eremias vermiculata* (Squamata: Lacertidae). *Mitochondrial DNA Part A*, **27**(2): 1447–1448.

Tseng SP, Li SH, Hsieh CH, Wang HY, Lin SM. 2014. Influence of gene flow on divergence dating – implications for the speciation history of *Takydromus* grass lizards. *Molecular Ecology*, **23**(19): 4770–4784.

Uetz P, Freed P, Aguilar R, et al. 2024[2024-12-21]. The reptile database. http://www.reptile-database.org.

van Etten J, Hijmans RJ. 2010. A geospatial modelling approach integrating archaeobotany and genetics to trace the origin and dispersal of domesticated plants. *PLoS One*, **5**(8): e12060.

Wang C, Wang XB, Liu DW, et al. 2014. Aridity threshold in controlling ecosystem nitrogen cycling in arid and semi-arid grasslands. *Nature Communications*, **5**: 4799.

Wang F, Sun DH, Chen FH, et al. 2015. Formation and evolution of the Badain Jaran Desert, North China, as revealed by a drill core from the desert centre and by geological survey. *Palaeogeography, Palaeoclimatology, Palaeoecology*, **426**: 139–158.

Wang IJ, Bradburd GS. 2014. Isolation by environment. *Molecular Ecology*, **23**(23): 5649–5662.

Wang Q, Zhang HX. 2022. Population genetic structure and biodiversity conservation of a relict and medicinal subshrub *Capparis spinosa* in arid Central Asia. *Diversity*, **14**(2): 146.

Wang Q, Zhang ML, Yin LK. 2016. Phylogeographic structure of a Tethyan relict *Capparis spinosa* (Capparaceae) traces Pleistocene geologic and climatic changes in the western Himalayas, Tianshan Mountains, and adjacent desert regions. *BioMed Research International*, **2016**: 5792708.

Wang Y, Zhao LM, Fang FJ, et al. 2013. Intraspecific molecular phylogeny and phylogeography of the *Meriones meridianus* (Rodentia: Cricetidae) complex in northern China reflect the processes of desertification and the Tianshan Mountains uplift. *Biological Journal of the Linnean Society*, **110**(2): 362–383.

Warren DL, Glor RE, Turelli M. 2008. Environmental niche equivalency versus conservatism: quantitative approaches to niche evolution. *Evolution*, **62**(11): 2868–2883.

Watanabe S, Hajima T, Sudo K, et al. 2011. MIROC-ESM 2010: model description and basic results of CMIP5-20c3m experiments. *Geoscientific Model Development*, **4**(4): 845–872.

Wright S. 1943. Isolation by distance. *Genetics*, **28**(2): 114–138.

Wu N, Wang S, Dujsebayeva TN, et al. 2023. Geography and past climate changes have shaped the evolution of a widespread lizard in arid Central Asia. *Molecular Phylogenetics and Evolution*, **184**: 107781.

Wu Z. 1981. Approach to the genesis of the Taklamakan Desert. *Acta Geographica Sinica*, **36**(3): 280–291. (in Chinese)

Xu R, Dujsebayeva TN, Chen D, et al. 2023. Phylogeography and ecological niche modeling of the Alashan pit viper (*Gloydius cognatus*; Reptilia, Viperidae) in Northwest China and adjacent areas. *Animals*, **13**(23): 3726.

Yang XP, Scuderi LA. 2010. Hydrological and climatic changes in deserts of China since the late Pleistocene. *Quaternary Research*, **73**(1): 1–9.

Yang XP, Scuderi L, Paillou P, et al. 2011. Quaternary environmental changes in the drylands of China – A critical review. *Quaternary Science Reviews*, **30**(23-24): 3219–3233.

Zan JB, Louys J, Dennell R, et al. 2024. Mid-Pleistocene aridity and landscape shifts promoted Palearctic hominin dispersals. *Nature Communications*, **15**(1): 10279.

Zhang HX, Zhang ML, Sanderson SC. 2013. Retreating or standing: responses of forest species and steppe species to climate change in arid Eastern Central Asia. *PLoS One*, **8**(4): e61954.

Zhang Q, Xia L, He JB, et al. 2010. Comparison of phylogeographic structure and population history of two *Phrynocephalus* species in the Tarim Basin and adjacent areas. *Molecular Phylogenetics and Evolution*, **57**(3): 1091–1104.

Zhang YJ, Stöck M, Zhang P, et al. 2008. Phylogeography of a widespread terrestrial vertebrate in a barely-studied Palearctic region: green toads (*Bufo viridis* subgroup) indicate glacial refugia in Eastern Central Asia. *Genetica*, **134**(3): 353–365.

Zhao H, Sun YB, Qiang XK. 2022. Mid-Pleistocene formation of modern-like desert landscape in North China. *CATENA*, **216**: 106399.

Zhou SZ, Wang XL, Wang J, et al. 2006. A preliminary study on timing of the oldest Pleistocene glaciation in Qinghai-Tibetan Plateau. *Quaternary International*, **154–155**: 44–51.

Zhou TH, Liu JL, Guo XG. 2016. Complete mitogenome of a variegated racerunner, *Eremias vermiculata*, from north of Tianshan Mountains, Xinjiang, China. *Mitochondrial DNA Part A*, **27**(4): 2765–2766.